Astronomy & Astrophysics manuscript no. output
February 27, 2018

SimCADO – The Instrument Data Simulator for MICADO at the ELT

I. The imaging modes

K. Leschinski[1], O. Czoske[2,1], G. Verdoes Kleijn[3], W. Zeilinger[1], J. Alves[1], R. Köhler[2,1], M. Mach[1], and S. Meingast[1]

[1] Department of Astrophysics, University of Vienna, Türkenschanzstr. 17, A-1180 Vienna, Austria
e-mail: kieran.leschinski@univie.ac.at
[2] Institut für Astro- und Teilchenphysik, Universität Innsbruck, Technikerstr. 25/8, A-6020 Innsbruck, Austria
[3] Kapteyn Astronomical Institute, University of Groningen, PO Box 800, 9700 AV Groningen, The Netherlands

Received 01.03.2018; accepted TBD

ABSTRACT

Context. When the Extremely Large Telescope comes online at the end of 2024, MICADO will be the near infrared imaging camera available at first light. As part of the design activities for MICADO we have developed SimCADO: an instrument data simulator in the form of a Python package. SimCADO produces simulated data frames for MICADO's 9 detector chip by applying the effects of each element along the optical train to a three dimensional (x,y,λ) description of the flux arriving from an astronomical object. Simulated images can be written to disk as FITS files and can be analysed by the standard suite of astronomical software.
Aims. The main aim of this study is to introduce the SimCADO software and to provide preliminary detection limits for MICADO to the community to aid others in preparing future science cases and observation strategies
Methods. To verify the accuracy of SimCADO we compared the characteristics of simulated images of globular clusters with images of the same clusters from the ESO archive. We then used a model of the current optical train design for MICADO to determine the sensitivity limits for MICADO at the ELT.
Results. SimCADO was able to accurately produce the image characteristics of raw archival HAWK-I data to within the limits of the model of the UT4/HAWK-I optical train. Using the current design of MICADO, SimCADO found detection limits in the J, H and Ks filters to be 28.7^{m}, 27.9^{m} and 27.3^{m} respectively for a 5σ detection in a 5 hour observation. This leads to the ability to observe for the first time with a ground based observatory individual A0 V stars at a distance of 4 Mpc (i.e. in Centaurus A), and M9 V stars in the Large Magellanic Cloud.

1. Introduction

Over the next decade the era of the extremely large telescopes will be begin. The European Extremely Large Telescope (ELT, Gilmozzi & Spyromilio 2007) will provide astronomers with the increase in resolution and sensitivity needed to solve many of the outstanding questions of modern day astronomy.

With a 39 m primary mirror consisting of 798 individually steerable 1.45 m hexagonal mirror segments and a fully deformable quaternary mirror, the ELT will be capable of providing diffraction-limited imaging with the help of the adaptive optics (AO) modules. This corresponds to a core full-width half maximum (FWHM) for the point spread function (PSF) in the J-band ($\sim$ 1.2 µm) of $\sim$ 8 mas and $\sim$ 14 mas in the Ks-band ($\sim$ 2.16 µm). Both single- and multi-conjugate modes for the adaptive optics will be possible. Laser guide stars (LGS) will be available to ensure that the ELT will always be able to provide AO-assisted observations.

As the first-light wide-field imaging camera for the ELT, MICADO – the **M**ulti-AO **I**maging **CA**mera for **D**eep **O**bservations (Davies et al. 2010) – will take advantage of the ELT's near-infrared optimised design to provide images at the diffraction limit. MICADO will provide a wide-field imaging mode and a zoom (narrow-field) mode with 4 mas/pixel and 1.5 mas/pixel plate-scales respectively. The detector plane will consist of nine 4096×4096 detector chips, allowing MICADO to cover a Field of View (FOV) of $\sim$ 55″ by $\sim$ 50″ in the wide-field mode and $\sim$ 21″ by $\sim$ 19″ in the zoom mode.

MICADO will also contain a series of additional modes, including: a long-slit spectroscopic mode with a spectral resolution of up to $R \sim 8000$, windowed high-time-resolution (HTR) imaging mode with a read-out speed of up to 250 Hz and a high-contrast imaging mode.

As the scale and complexity of telescopes and instruments increases, so too does the importance of accurately being able to predict the performance of these systems. More and more emphasis is being placed on developing simulation software to model all aspects of new instruments before they enter the construction phase. As part of the development of the MICADO instrument, the Data Flow Systems work package within the MICADO consortium has been tasked with creating a tool to simulate raw detector read-out images based on the current designs of the ELT and MICADO. Here we present SimCADO, the instrument data simulator for MICADO. SimCADO combines the most recent data from the other work packages in the consortium to allow the user to simulate the above mentioned raw data frames that will be produced by the ELT/MICADO optical system.

In this paper we introduce the SimCADO package and show that it is a useful tool for producing not only accurate simulated images for the MICADO/ELT optical system, but also for any other optical train, such as for HAWK-I on UT4 at the VLT. This paper is organised in the following way: Sect. 2 delves briefly into the motivation behind creating SimCADO as well as giving an overview of the scope of the project. The physical effects that SimCADO models are described in Sect. 3. A description of how we validated SimCADO by comparing sim-

ulated VLT/HAWK-I read-out frames to real images from the ESO archive can be found in Sect. 4 and predictions for the sensitivity of the ELT/MICADO system are presented in Sect. 5. A discussion of the results, assumptions and issues with the simulated images is presented in Sect. 6.

2. SimCADO – the Python package for simulating MICADO imagery

2.1. Motivation and Scope

The scientific return of instruments like the ELT and MICADO is the primary reason for building such complex pieces of machinery. Knowing in advance what the capabilities of an instrument will be, and preferably knowing just how well the instrument will perform for different configurations is invaluable during the design phase. Furthermore, MICADO and other instruments like it (e.g. HARMONI, Thatte et al. 2010; METIS, Brandl et al. 2008; etc.) are built by trans-national consortia, with many members from different institutes in different countries. As such the nodes in the consortia enjoy a certain level of geographic displacement. Each node in the consortia therefore often defaults to generating their own simulated data for the task to which they have been assigned. Additionally, the end users of the instrument also want to know how the instrument will behave and how useful it will be for their personal scientific projects well in advance so that they may prepare for when the instrument becomes available. All of these points can be considered true for almost all large instrument projects in modern day science – hence why there has been a very concerted effort by the scientific community, and very notably by the astronomical community to develop full scope instrument data simulators for major projects (see e.g. HSIM for ELT/HARMONI, Zieleniewski et al. 2015; the ELT/METIS simulator, Schmalzl et al. 2012; PhoSim for the LSST, Peterson et al. 2015; TOAD for 4MOST, Winkler et al. 2014; WebbPSF for JWST, Perrin et al. 2015; IRIS Data Simulator for TMT, Wright et al. 2016; etc.).

2.2. The SimCADO audience

We have developed SimCADO for use primarily within the MICADO consortium, but also for interested external parties. SimCADO's main strength is that it gives all members of the consortium a common tool to generate simulated data for their assigned tasks. Among the consortium we see the main user groups being:

The science team: During the current design phase the science team members are running feasibility studies to determine which science cases are the biggest drivers for the design of the instrument. By using a common tool to generate simulated images, the science team, and those using the findings of the science team to make design decisions, can be confident that the results are all comparable.

The data reduction pipeline: In order to create a reliable set of reduced data products which are available from the beginning of operations, the data reduction pipeline must be developed before the first data are collected. SimCADO takes into account all processes that affect the incoming light as is travels from the source to the detector. As such it is perfect for generating so-called "dirty" images which can be used as fake input for the reduction pipeline. By using such images, the majority of coding for the reduction pipeline can happen without the need for the instrument to already be operational.

The data archive: The ability to produce simulated data also allows the development of a data archive to proceed prior to the availability of real data. SimCADO images will be used to help define the data products offered by MICADO and the method of storage and retrieval well before the instrument generates any images of its own accord.

Instrument design team: SimCADO relies heavily on input from the different consortium work packages in order to produce images representative of the whole instrument. This in turn means that, by providing multiple sets of input data for a specific component in the optical train, a work package can use SimCADO to test the effect of different component designs on the final image quality. By using a standard set of science cases and weighting the importance of each aspect of the various science cases, trade-off analyses can be conducted. It should however be noted that SimCADO does *not* follow individual photons through the optical train. It assumes large numbers of photons and uses expectation values for photon intensities over the whole field of view. We therefore recommend that further investigation for design trade-offs should be undertaken with other more in-depth methods (e.g. using ray-tracing software like ZEMAX) before any final decision is made.

Observation preparation software: Given the capabilities and expense of the ELT/MICADO system, observation time will be costly and in high demand. Therefore it is prudent to optimise observations to get the most out of any time on-sky. Currently, exposure time calculators are provided to assist in observation preparation. However, given the myriad of celestial environments encountered during observations, single numbers based on look-up tables are often not enough to accurately predict exposure times. For the ELT/MICADO system, integrating SimCADO into the preparation software will allow the user to not only determine the required exposure time, but also to visualise and assess the effect of surrounding objects on the detectability of the target object. This should help to reduce the number of non-detections during actual observations, and therefore increase the scientific output of the MICADO and the ELT.

The MAORY consortium: MICADO will be the first and main beneficiary of the MAORY AO module (Diolaiti 2010). Consequently the development of the MAORY module is inextricably linked to MICADO. Design choices made in the MAORY consortium will have a direct impact on the quality of the science that MICADO will be able to produce. By using SimCADO, members of the MAORY consortium will also be able to see directly how these design choices will affect MICADO observations.

The astronomy community at large: Although first-light for the ELT is slated for 2024, preparation work needs to begin well in advance so that the astronomical community can "hit the ground running" once the ELT and MICADO are online. Many of the ideas that will be tested post-2024 will need to be developed over the coming years. It is therefore important that the astronomical community have a tool that enables new ideas to be thoroughly tested, and where necessary, preparation observa-

tions to be conducted, before applying for time with MICADO. SimCADO can help test the feasibility of observations for new ideas.

2.3. SimCADO as an Instrument Data Simulator

First and foremost SimCADO was conceived as an instrument data simulator (IDS), not an end-to-end (E2E) simulator. An IDS differs from an E2E simulator in the following way: an E2E simulator models the interactions between each object and each element in the optical train with the incoming photons in a physically realistic manner, i.e. taking into account the physical interactions between photons and computer representations of physical objects along the optical train (see photon-tracing in PhoSim for the LSST: Peterson et al. 2015). An IDS, on the other hand, turns the effects of each element in the optical train into mathematical operators, which are then applied to an input "image" (a 2D/3D representation of the sky). IDSs require much less computation power and are therefore much better suited for quick, personalised simulations and prototyping. However, this comes at the cost of flexibility. E2E simulations can create images for any physical configuration of the optical train, as long as a physical model of all components exist in memory. IDSs only generate output for a certain configuration if data (often originally created by an E2E simulation) already exists and can be converted into a series of mathematical operators. A good example is the case of the PSF. Given a point source with a certain brightness, the PSF will appear on the focal plane of an E2E simulation by only supplying a model of the physical objects along the light's path (spiders, mirrors, pupil stops, etc.). An E2E simulator needs only the values pertaining to the physical positions and dimensions of these objects. An IDS on the other hand is able to project a PSF onto the focal plane because a mathematical description (either a 2D image array or a 2D function) of that PSF has been supplied. The IDS then convolves this description with one or many point sources. Regardless of how the optical train changes, unless this mathematical description has been updated from another source (i.e. output from a separate E2E simulator) the IDS images will continue to display the same PSF.

The main advantage of developing and using an instrument data simulator lies in its speed and ease of use. Because IDSs rely on the results of other simulations, IDS simulations are many orders of magnitude faster than those conducted with E2E simulators. Our main goal with SimCADO was to provide a tool that gives the casual user the ability to simulate images for MICADO in a matter of minutes on their own laptop. Such an approach is advantageous to both the user and the developer when compared to the alternative model: the user must submit a simulation request to a dedicated "simulations" team. With SimCADO running on the user's laptop, both the time the user must wait for results and the work load of the simulations team are drastically reduced. This in turn allows the simulations team to direct their efforts towards improving the software and keeping the instrument configuration up to date.

Further justification for concentrating our efforts on an IDS rather than an E2E package comes from the fact that for the majority of cases (excluding those from the design team), the optical train stays exactly the same. Therefore there is no need to re-simulate from scratch each and every photon interaction (as an E2E simulator would do) every time a simulation is run.

3. The physical effects modelled by SimCADO

SimCADO takes into account all effects between the light source and the detector. This includes the atmosphere, the telescope, the instrument, and the detector array. We have designed SimCADO in such a way as to allow any optical train to be modelled, providing all the relevant data is available[1]. The default configuration is for the ELT/MICADO optical train. For testing purposes we have configured SimCADO to reproduce the effects of the VLT/HAWK-I optical train (see Sect. 4). In this section we describe the effects of the optical elements that the current version (0.4) of SimCADO takes into account.

For a full description and discussion of the internal workings of the SimCADO package, the reader is directed to the paper by Leschinski et al. (2016) and to the online SimCADO documentation.[2]

3.1. Atmosphere

Transmission and Emission: The SkyCalc tool[3] (Noll et al. 2012; Jones et al. 2013) provides accurate spectral models of the atmospheric transmission and emission (see Fig. 1 for the transmission and emission curves). For SimCADO we have taken the default model, which uses atmospheric conditions averaged over the whole year and a unity airmass. In a future release we hope to include the functionality to query the SkyCalc server directly from within SimCADO. However until such time, if the user is interested in investigating the effects of different atmospheric conditions on the resulting detector output, SimCADO accepts ASCII text files generated by the online SkyCalc tool as input for simulation runs.

As an alternative to using the default spectral energy distribution provided by SkyCalc, the user may instruct SimCADO to use a certain sky background emission for a given broadband magnitude in mag/arcsec^2.

Atmospheric diffraction: For effects that act along all three relevant simulation dimensions (x, y, λ) SimCADO uses an adaptive layered approach. Briefly this means that SimCADO determines how separated in spectral space two individual monochromatic images can be before a noticeable spatial shift between two adjoining layers occurs. This parameter can be set in the SimCADO configuration file. By default a new spectral bin is created once the shift due to the atmospheric dispersion is greater than one pixel (i.e. 4 mas and 1.5 mas in the wide-field and zoom modes, respectively). The spatial shifts induced by the atmosphere are calculated according to the formulae from Stone (1996) and from the review by Pedraz[4]. In order to avoid unnecessarily increasing the computational workload, any shifts induced by the atmospheric dispersion are inversely scaled according to the performance parameter for the atmospheric dispersion corrector (ADC). By by default this is set to 100 % – i.e. no atmospheric dispersion is included.

PSF variability : SimCADO does not create atmospheric point spread funtions (PSFs) on the fly. Instead it requires a PSF to be

[1] We have also created configuration packages for the HST+WFC3 system and the VLT/HAWK-I systems.
[2] http://www.univie.ac.at/simcado
[3] https://www.eso.org/observing/etc/bin/gen/form?INS.MODE=swspectr+INS.NAME=SKYCALC
[4] http://www.caha.es/newsletter/news03b/pedraz/newslet.html

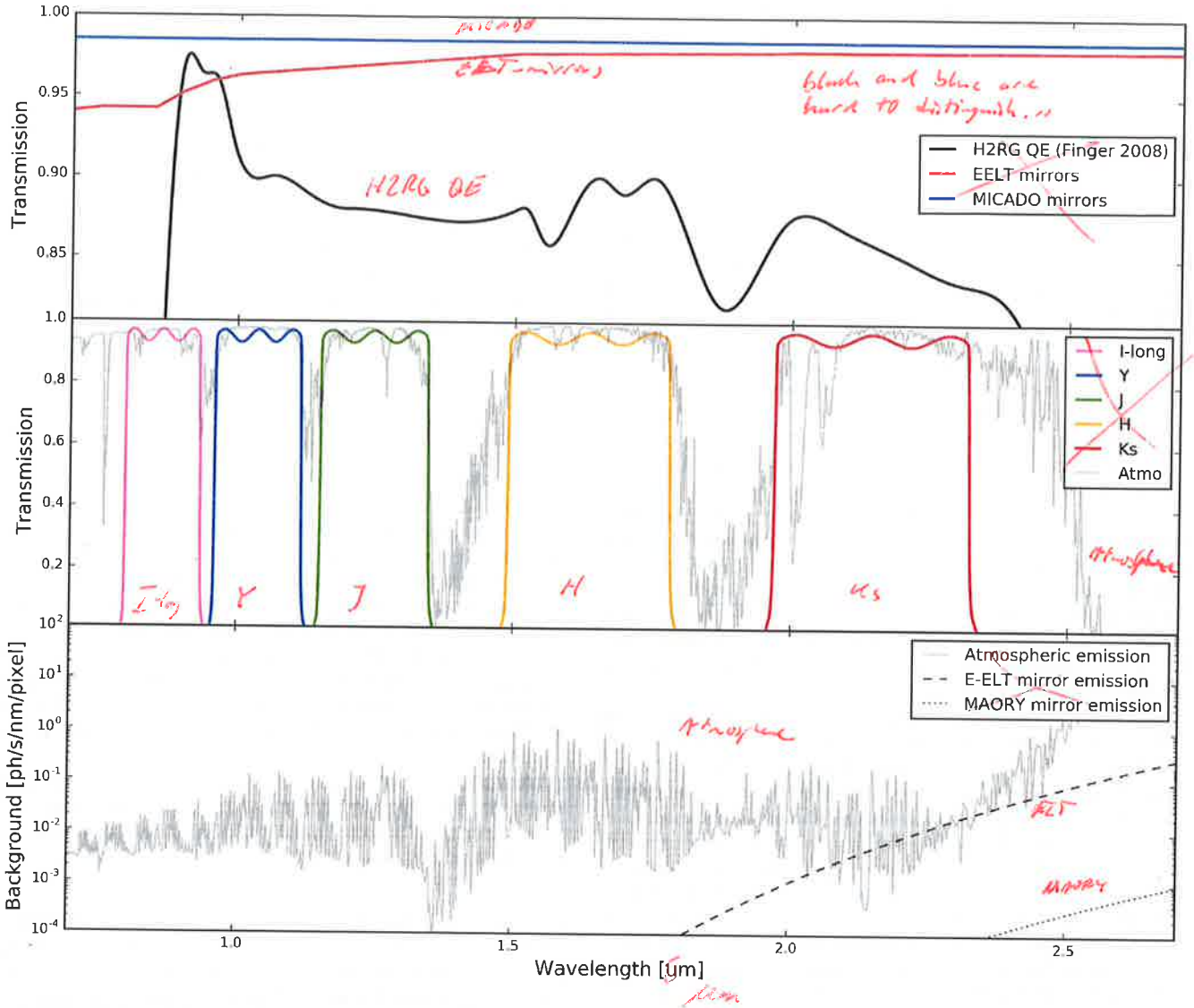

Fig. 1. Default transmission and emission curves used by SimCADO. Top: The mirror transmission curves for both the ELT and MICADO plotted together with the quantum efficiency (QE) curve for the HAWAII 2RG detectors. The ELT will use a AgAl mirror coating with a MgF_2 protective layer (Boccas et al. 2006) while the 14 MICADO mirrors will be gold coated (Davies et al. 2016). SimCADO uses the QE curve for the H2RG detectors because this information for the H4RG detector is not currently available to the public. As soon as the QE curve for the 4k detectors becomes available, the SimCADO defaults will be updated. Middle: A selection of broadband filters for MICADO (IYJHKs) based on projected filter properties. SimCADO ships with a collection of curves for the filters currently foreseen for use in MICADO. The atmospheric transmission curve used by SimCADO was generated by the skycalc tool (Noll et al. 2012; Jones et al. 2013) and can be adjusted for zenith distance. Bottom: the photon background flux per MICADO wide-field mode pixel (i.e. 4 mas) coming from the atmosphere and from the ELT and MAORY mirror grey-body emission. The units are photons per second per nanometer calculated for the full area of the ELT's mirrors. The sky background emission spectrum was generated using the skycalc tool with the default parameters. The ELT mirror emission is for an ambient dome temperature of 0 degrees Celsius and combines the emission from all five of the ELT's mirrors. The MAORY mirror emission is assuming warm optics at the dome temperature and the optical train as detailed by Diolaiti (2010) and Diolaiti et al. (2016). The total area of the MAORY mirrors is taken to be 3.4 m^2.

provided, either by the other teams working in conjuction with the MICADO consortium (i.e. the SCAO and MCAO simulation teams) or by the user. PSFs will be discussed in greater detail in Sect. 3.2; however, it is worth mentioning here that SimCADO provides a series of functions for generating "ELT"-like PSFs based on the POPPY PSF simulation package (Perrin et al. 2015). The function `simcado.psf.poppy_ao_psf()` allows the user to specify the level to which the seeing halo is added to an ideal diffraction limited PSF, thus allowing the user to create PSFs for different seeing conditions.

Currently SimCADO does not automatically include time variability in the PSF or in the atmospheric parameters. However, SimCADO's implementation in Python allows the user to script many different simulation configurations, thus providing the functionality to implement temporally varying atmospheric conditions. An automated method for doing this is foreseen for later releases of SimCADO.

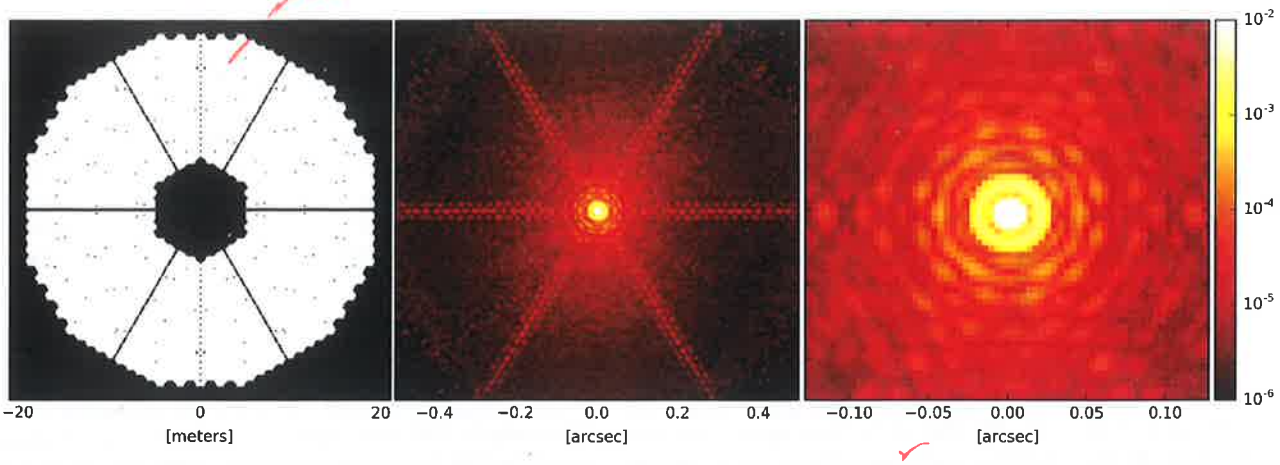

Fig. 2. Left: the ELT pupil with the full mirror configuration, not taking into account any circular obscuration in subsequent pupil planes. Middle: the current SCAO PSF used by SimCADO as developed by Clenet et al. (2013). The PSF has a Strehl Ratio of 68 % in the Ks band over a 4″ FoV. The effects of a segmented mirror on the diffraction spikes are clearly visible. Right: a cutout of the central 0.25″ of the PSFs. The effect of the segmented mirror is also present in the structure of the Airy rings around the core of the PSF.

3.2. The ELT

Point Spread Function: Being an IDS, SimCADO does not need to know how the PSF is generated or what happened to it before the instrument focal plane. All SimCADO needs is the total (wavelength dependent) effect of the whole optical train on the spatial distribution of light on the focal plane. How the atmosphere deforms the PSF and how the AO modules correct for this are outside the scope of SimCADO. Only the net effect of the two counteracting operations are important for simulations.

Currently the two adaptive optics (AO) modes that will be offered with MICADO are:

- single conjugate (SCAO, Clénet et al. 2016), which will provide diffraction-limited imaging with Strehl ratios of > 60 % in Ks-band in the centre of the field of view.
- multi-conjugate (MCAO) in conjunction with the MAORY module, which will provide diffraction-limited imaging of the full MICADO field of view with Strehl ratios between 30 % and 50 % in Ks band (Diolaiti et al. 2016)

Currently, SimCADO only provides a SCAO PSF from the E2E simulation efforts of Clénet et al. (2015, obtained via private communication). MCAO PSFs will be included as soon as the MAORY consortium releases them for public use. Currently, the PSFs do not take into account variability over the FoV. This effect will be included in a later release of the simulator.

In addition to the PSFs provided by the E2E AO simulations, SimCADO also provides functionality to generate lower fidelity PSFs using an analytical model. This model is not as accurate as the E2E simulations but it does allow the user to conduct comparative studies. For example, the user can investigate how different Strehl ratios will affect the results for a certain science case. The analytical PSF is generated by summing two weighted PSFs, a diffraction-limited PSF and a seeing-limited PSF, according to the equation:

$$\mathrm{PSF}_{\mathrm{Analytical}} = \mathrm{SR} \times \mathrm{PSF}_{\mathrm{Diffraction}} + (1 - \mathrm{SR}) \times \mathrm{PSF}_{\mathrm{Seeing}}, \quad (1)$$

where SR is the desired Strehl ratio, $\mathrm{PSF}_{\mathrm{Diffraction}}$ is the diffraction-limited PSF generated by the POPPY package (Perrin et al. 2015) for a 39 m diameter segmented mirror with six support beams for the secondary mirror (see Fig. 2), and $\mathrm{PSF}_{\mathrm{Seeing}}$ is a PSF following a Moffat profile with a full width half maximum (FWHM) corresponding to the seeing limit of the observations. For the seeing-limited PSF, SimCADO uses a FWHM of 0.8″ by default. The default Strehl ratio for the analytical PSF is set to the Strehl ratio that MAORY is required to provide, i.e. 30 % in K band and 12 % in J band (Diolaiti et al. 2016). Currently, SimCADO does not vary the shape of the PSF over the field, as would be consistent with AO observations. We are however developing this functionality for a future release

Transmission and emission: SimCADO uses the reflectivity curve provided by the ESO Data Reference Mission (DRM) for the ELT[5] for an aluminium-silver mirror coating with a magnesium flouride protective layer (AgAl-MgF_2). This is currently the preferred mirror coating for all five of the ELT mirrors. For comparison SimCADO also provides the transmission curve for a pure aluminium coating (as used at the VLT). The reflectivity in the near infrared regime is almost constant at ~ 98 %.

The grey-body emission for the ELT is calculated by assuming all emission is coming from a single surface with the combined area of all five mirrors (~ 1030 m^2) and at a temperature of 0 degrees Celsius. This light is subject to the transmission losses of all five ELT mirrors. While this is not a completely correct representation of what happens to the grey-body emission – light from M1 is subject to reflectivity losses from 4 mirrors, while there is no loss of emitted light from M5 due to ELT surfaces – because of the shear size of M1 (~980m^2) the difference in total grey-body light from the five ELT mirrors is < 0.15%. **(OC: But this has been implemented correctly a long time ago!)** This source of uncertainty is far outweighed by the uncertainty in the assumed temperature of the mirrors. The increase in computation speed by only using one characteristic transmission curve for the grey-body emission is noticeable and justifies this approximation.

Wavelength independent spatial effects: Effects related to unwanted movements of the telescope are also built into SimCADO. Wind jitter and vibrations due to the cooling equipment introduce a further blurring term into the image. This can be

[5] https://www.eso.org/sci/facilities/eelt/science/drm/

Sect. 3 kann sich nicht entscheiden, ob es eine vollständige Darstellung von SimCADO sein will, oder nur eine Übersicht, um einen eigenen Zweck dieses Papers zu dienen.

Table 1. The root-mean-square wavefront error expected for each surface in the MICADO optical train. The total wavefront error is expected to be on the order of 76 nm, which translates to a decrease in PSF peak strength of ~ 5 % at 2.2 µm ~ 14 % at 1.25 µm (R. Davies, private communication)

Wavefront error rms [nm]	Surfaces	Material	Optical element
20	11	gold	Mirror
10	4	glass	Entrance window
10	2	glass	Filter
10	8	glass	ADC

modelled by convolving the final focal plane image with a 2D Gaussian distribution. The FWHM of the Gaussian is a function of the strength and frequency spectrum of both the vibrations and the wind. At this stage we have assumed that the ELT's vibration damping mechanisms will remove the vast majority of vibrations. As such default vibrations in SimCADO are set to a FWHM of 0.001″, thus removing this effect from the default simulations.

SimCADO provides the functionality to simulate the smear introduced by sub-optimal mechanical performance of the ELT's tracking system. However a quick back-of-the-envelope calculation shows that the update frequency of the ELT's stepper motors needs to be on the order of 10 – 100 kHz if the sky is to move less than a MICADO pixel length between updates. This is well within the scope of modern day stepper motor technology and so by default SimCADO assumes that the ELT's tracking system will not cause noticeable image smearing.

3.3. MICADO

We have developed SimCADO during the preliminary design phase of MICADO. The default configuration for SimCADO is continually updated to reflect the most recent design of the instrument. Values presented in this subsection are correct at the time of publication, but need not be identical to those in the most recent version of the SimCADO package. See Davies et al. (2016) for the MICADO design at the time of writing.

Transmission: SimCADO takes into account all optical surfaces along the instrument optical train including: the cryostat entrance window (4 surfaces), the internal fold mirrors, the atmospheric dispersion corrector (4 prisms, 8 surfaces), the zoom optics, the filters (2 surfaces) and the pupil placeholders. Additional surfaces needed for the spectroscopy mode include the entrance slit and the grisms. These will described in a companion paper on the SimCADO spectroscopy mode.

Currently by default all the mirrors are assumed to be coated with gold with a reflectivity of 98.5 % across the whole spectral range. SimCADO also ships with all common visual and NIR broadband filters (UBVRIzYJHKKs) and a series of common narrow band filters for NIR observations, taken from the Spanish virtual observatory database[6]. The user is also able to direct SimCADO to use any filter curve for which they have an ASCII file containing wavelength and transmission values by using the `TransmissionCurve` object. See the SimCADO documentation for more information.

[6] `http://svo2.cab.inta-csic.es/theory/fps3/index.php?mode=browse`

Non Common Path Aberrations (NCPAs): The default PSFs do not take into account the NCPAs due to the difference in optical path to the wave-front sensors and to the detector array. Characterising the MICADO NCPAs is still an active topic. We will include both the spatial and spectral effects of the NCPAs in a later release of SimCADO once a model exists to describe them. In the meantime we are able to use wave-front error budgets to determine an approximate wavelength dependent reduction in the peak intensity, $\Delta f_{\rm peak}$, of the PSF due to the NCPAs according to Eq. (2):

$$\Delta f_{\rm peak} = e^{-(2\pi \mathrm{WFE}_{\rm total}/\lambda)^2}, \quad (2)$$

where $\mathrm{WFE}_{\rm total}$ is the total wavefront error expected for all NCPAs along the MICADO optical path and λ is the wavelength for which the PSF has been constructed. Table 1 details the individual wavefront errors that SimCADO uses to calculate $\mathrm{WFE}_{\rm total}$. The total wave front error is expected to be on the order of 76 nm which translates to a decrease in PSF peak strength of ~ 5 % at 2.2 µm, and ~ 14 % at 1.25 µm (R. Davies, private communication).

Atmospheric Dispersion Corrector (ADC): Like the PSF, the effect of atmospheric dispersion is visible in all three instrumental dimensions (x, y, λ). In order to simulate this effect SimCADO creates a series of monochromatic image slices for a series of spectral bins within the filter wavelength range (see Leschinski et al. 2016 for a detailed description of how SimCADO does this). The bin width is chosen in such a way that the elongation induced by the atmospheric dispersion is never greater than one pixel (i.e. 4 mas in wide field mode, or 1.5 mas in zoom mode). If the ADC is working perfectly then the atmospheric dispersion is completely removed and the spectral bin width is equal to the full width of the filter. If the ADC is turned off, the relative shift of an image over the full J-band is around 0.19″, or almost 50 wide-field pixels, at a zenith distance of 60 degrees. To maintain a relative shift per monochromatic image slice of less than a single pixel, SimCADO must generate almost 50 monochromatic slices, each shifted relative to the reddest slice. By stacking all the slices (including shifts) on the detector plane the dispersion caused by the atmosphere can be reproduced in the final output image. By default SimCADO assumes that the ADC is working perfectly and so does not need to introduce any extra image slices. Once the design of the ADC progresses and the residuals of the correction are quantified, we will update the default parameters for SimCADO to reflect this.

Derotator: A perfectly functioning derotator is essential for maintaining the astrometric accuracy of sources near the edges of the detector plane. Similar to the ADC we have implemented the effect of a less-than-perfect derotation by combining a series of image slices for which the shift at the edge of the detector array is less than one pixel. However as the sky rotation is a purely spatial effect, the image slices are generated for temporal bins (i.e. a series of short "exposures"), as opposed to the spectral bins for the ADC (again, see Leschinski et al. 2016 for further details). By default, SimCADO assumes perfect derotation, but as always the defaults will be updated as soon as more information becomes available.

Instrumental Distortion: Another effect that is important for accurate astrometric measurements is the instrumental distortion.

zu viel "currently" – in SimCADO kann man die Daten flexibel ändern. Vielleicht sind diese Festlegungen besser auf die photometrische Studie – "for the purposes of this paper" ... "in this study" ...

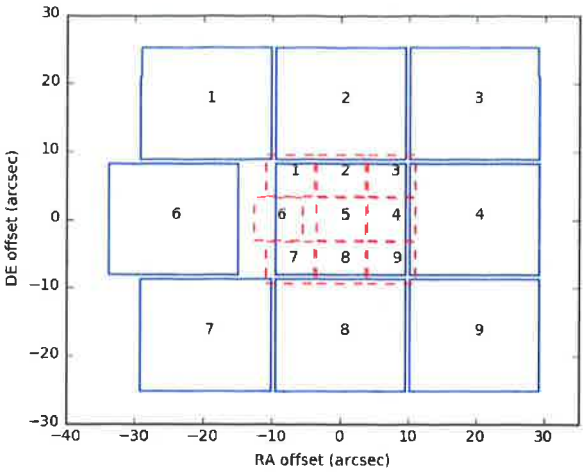

Fig. 3. The footprints of the two imaging modes for MICADO. The wide-field mode (solid lines) has an on-sky footprint of ~ 55″ × 50″, while the zoom mode (dashed lines) has an on-sky footprint of ~ 21″ × 19″. The H4RG will only be 3-side buttable due to the placement of the read-out electronics, the result of which is the extended gap between chips 5 and 6 in the middle row.

Although not included in the publicly available version of SimCADO at the time of writing (version 0.4) this functionality is currently being developed and will be included in future releases of the package. The implementation of the instrumental distortion will be discussed in a companion paper detailing the spectroscopic capabilities of SimCADO.

3.4. MICADO Detector Array

The current design for MICADO includes a 3 × 3 array of HAWAII-4RG chips (Davies et al. 2016). SimCADO takes into account the positions of the chips on the focal plane as well as the gaps between the nine chips, the electronic noise characteristics of the HAWAII chips as well as the linearity of the chips. Detailed information is not publicly available and so we have based the detector characteristics primarily on the H2RG chips, the predecessors to the H4RGs.

Electronic noise: Rauscher (2015) created the python package NGHxRG[7] to simulate read noise frames for the HAWAII-2RG detectors used in the JWST NIRSpec instrument (Posselt et al. 2004). SimCADO uses this package to create noise frames for the HAWAII-4RG detector series. Included in the noise frames are: white (read) noise, residual bias drifts, pink $1/f$ noise and alternating column noise. Picture frame noise can also be included, however as there are not yet any estimates for MICADO, SimCADO bases its picture frame noise on the default file provided by the NGHxRG package. The default parameters used when generating the noise frames are given in default configuration file in Appendix B.1.

Detector gaps: In its base configuration, the MICADO detector plane will consist of 9 H4RG detectors, each covering slightly more than 16″ × 16″ on sky. Because of the read-out electronics, each chip will only be 3-side buttable, meaning that one of the eight outer chips must be placed further from the central chip than its counterparts. This can be seen in on-sky footprints of the zoom and wide-field modes in Fig. 3. SimCADO contains configuration files detailing the positions of the detector chips for each of these base modes.

Linearity, Saturation, Persistence and Cross-Talk: Because detailed data on the H4RG chips are not yet publicly available, we have assumed that they will have a similar performance to the H2RG chips which are found in many current NIR instruments (e.g. VLT/HAWK-I, JWST/NIRSpec). The data for the linearity curve and saturation limits have therefore been taken from the HAWK-I detector array. As persistence and pixel cross-talk are more complex to model, SimCADO does not currently simulate these two effects. We plan to implement them in a later version of SimCADO.

Read-out schemes: SimCADO currently has two functions for reading out the chips on the detector array: "non-destructive" and "super-fast". The non-destructive mode mimics the functionality of the HAWAII-4RG chips, which allows the user to measure the pixel values without actually destroying the content of the pixels. This mode allows any non-destructive read-out scheme to be implemented, including the commonly used Fowler, double-correlated or up-the-ramp schemes. However, this mode is not the default and the scheme must be defined by the user.

Because the shortest exposure time for the default mode for MICADO observations is 2.6 s, observations will be background limited. Thus it is superfluous to calculate the read noise of each frame. Instead, by default, SimCADO uses the so-called "super-fast" read-out mode. The "super-fast" mode does not read out a series of single exposures every 2.6 s, rather it creates a single read-out with an exposure time equal to the duration of the full observations (i.e. `EXPTIME = NDIT*DIT`). Shot noise in the image scales as the square root of the total observation time. It is no surprise that the super-fast mode is NDIT times faster than the non-destructive read-out mode. For observations using super-fast which are greater than ~ 10 minutes, we recommend "turning off" SimCADO's detector linearity functionality so that the signal increases linearly with exposure time over the full duration of the observation. In future releases this will occur automatically based on the chosen mode.[8]

4. Validating SimCADO with raw HAWK-I data

Aside from testing during the coding phase, we tested the accuracy of SimCADO by comparing simulated raw detector readout images to raw observations from HAWK-I on UT4 at the VLT. HAWK-I, the High Acuity Wide-field K-band Imager (Kissler-Patig et al. 2008), is a present-day analogue to MICADO's imaging modes and thus a good test-bed for these comparisons. We created a configuration file that reflects the UT4/HAWK-I optical train from the publicly available instrument data on the ESO website[9] and from HAWK-I calibration data from the ESO archive to create a version of SimCADO that simulates raw ob-

[7] `http://jwst.nasa.gov/resources/nghxrg.tar.gz`

[8] It should be noted that regardless of the status of the detector linearity, there is still a hard limit of $2.14 \cdot 10^9$ photons per pixel set by numpy's "poisson" function. Larger values raise an error message. Hence all pixel values above $2.14 \cdot 10^9$ are capped so that shot noise can still be applied to the image.

[9] `http://www.eso.org/sci/facilities/paranal/instruments/hawki.html`

servations from HAWK-I. SimCADO then "observed" the globular clusters M4 and NGC 4147. We compared background flux levels and the photometry of stars in both the raw HAWK-I and simulated SimCADO images to gauge the accuracy of the simulations.

4.1. Modelling HAWK-I with SimCADO

To create a model of the HAWKI optical train, SimCADO required the following data:

- an estimate of the Point Spread Function (PSF) for the whole VLT/HAWKI system,
- transmission/reflectivity curves for each of the surfaces along the optical path,
- and details of the HAWKII-2RG detector characteristics

Additionally, a description of the globular clusters to be observed was needed. Creating the source description is described in more detail in Sect. 4.3.

The PSF: The seeing-limited nature of the UT4/HAWK-I optical train greatly simplified simulations. The combined system PSF could be, to a very good approximation, described by a diffraction limited Moffat profile for the round monolithic mirrors of the UT4 telescope (Dierickx et al. 1990) combined with a Gaussian profile for the atmospheric contribution. To include the effect of the "spiders" that are part of the support structure for the secondary mirror, we used the POPPY package to generate a diffraction limited PSF for an 8.2 m circular aperture with a 1.1 m secondary obscuration and four 0.1 m support beams. We then convolved this diffraction-limited PSF with a 0.5″ Gaussian to mimic the seeing-limited nature of HAWK-I observations. This artificial PSF can be see in the bright stars in Fig. 7.

Transmission curves for the optical train: The combined optical train of HAWK-I and the VLT's UT4 contains 7 aluminium-coated mirrors, an entrance window, a series of standard NIR filters and a detector plane with 4 HAWAII-2RG chips. The transmission, reflectivity and quantum efficiency curves for each of these elements were combined in SimCADO. The resulting transmission curve has an average transmission value of 0.52, which is very similar to the average value of 0.5 assumed by the online exposure time calculator provided by ESO.[10]

The detector array: Four HAWAII-2RG chip (Loose et al. 2007) are used in HAWK-I. The detector noise was generated internally by SimCADO using the NGHxRG package (Rauscher 2015). The quantum efficiency curve was taken from Finger et al. (2008). The detector linearity curve was extracted from the archive images. It was determined by fitting Gaussian profiles to the wings of a series of saturated stars in the raw observations and comparing the theoretical height of the best-fit Gaussian profile to the actual pixel values in saturated regions. The plate scale used by SimCADO was 0.106″.

Instrumental distortion was neglected because its effect was minimal when determining the photometric accuracy of a simulated stellar field. The flat field effect of the whole system was also neglected for this study. This was under the assumption that it will not drastically affect the photometric accuracy of the majority of stars in any simulated field.

[10] https://www.eso.org/observing/etc/bin/simu/hawki

Table 2. Limiting magnitudes calculated for HAWK-I from images generated by SimCADO, the ESO ETC and taken from Kissler-Patig et al. (2008). The SimCADO limiting magnitudes were calculated based on a 5σ detection in a grid of 100 stars with magnitudes spread linearly between 14^m and 27^m in the respective filters. The FWHM for the SimCADO PSF was chosen to match the "Image Quality" parameter given by the ETC. For a seeing value of 0.8″ in V band and an airmass of 1.2, the resulting FWHM for J, H and Ks (Brγ) band respectively was 0.62″, 0.58″, 0.53″.

Filter	Exposure	SimCADO	ETC	KP+2008
J	1 hr	23.8^m	24.2^m	23.9^m
	1 min	21.5^m	22.0^m	
	2 sec	19.7^m	20.1^m	
H	1 hr	22.7^m	23.3^m	22.5^m
	1 min	20.5^m	21.0^m	
	2 sec	18.8^m	19.2^m	
Ks	1 hr	21.9^m	22.2^m	22.3^m
	1 min	19.7^m	19.9^m	
	2 sec	17.8^m	18.1^m	
Brγ	1 hr	21.6^m	20.9^m	
	1 min	19.5^m	18.7^m	
	2 sec	17.5^m	16.8^m	

It should be noted that we are in the process of conducting a further study to quantify the extent to which different atmospheric conditions affect the accuracy of images generated with SimCADO. For this study we were granted 5 hours of technical time on HAWK-I and will report on the results in a future paper.

4.2. HAWKI-I Sensitivity with SimCADO

As a first test we compared the limiting magnitudes of images generated with SimCADO to both the limiting magnitudes given by Kissler-Patig et al. (2008), and those given by the exposure time calculator (ETC) on the ESO website. Table 2 shows that the limiting magnitudes for SimCADO in the J and H filters are within 0.2^m of the values given by Kissler-Patig et al. (2008), although there is a $\sim 0.5^m$ discrepency between SimCADO and the ETC. In the Ks filter the discrepancy is only $\sim 0.3^m$. The Brγ filter shows the biggest deviation of $\sim 0.7^m$. The observation parameters used in SimCADO were set to be identical to those described by Kissler-Patig et al. (2008), namely: seeing of 0.8″ in V-band and an airmass of 1.2. Fig. 4 shows the evolution of several relevant detection limits (e.g. 5σ for photometry, $\sim 250\sigma$ for astrometry) for HAWK-I as determined by SimCADO.

4.3. Comparison of SimCADO images with real observations

To test how well SimCADO reproduces the spatial aspects of an observation, we downloaded four raw FITS files of the popular globular clusters M 4 and NGC 4147 from three different observing runs conducted between 2007 and 2015 from the ESO archive. Table 3 lists the main parameters of these observations. Globular clusters by virtue of their age contain very little gas or dust and hence essentially no star formation activity. This makes them easy objects to model for SimCADO. We chose this series of raw images to test the performance of SimCADO over multiple observing configurations.

In order to simulate the raw images we generated SimCADO-readable `source` objects for the globular clusters M 4 and NGC 4147 using the 2MASS sky coordinates and appar-

Table 3. The raw HAWK-I data from the ESO archive used in this study. The three observations of M 4 were used to test the photometric accuracy of SimCADO under the assumption that the background level should remain similar. The observation of NGC 4147 was used to test the background flux under different exposure lengths.

ESO archive filename	Filter	Exposure [s]	V-band seeing [arcsec]	Airmass	Object
HAWKI.2015-06-10T05_12_28.683.fits	Ks	10	0.9	1.05	M 4
HAWKI.2007-08-05T01_34_45.908.fits	Ks	10	NA	1.05	M 4
HAWKI.2007-08-05T23_14_33.748.fits	J	10	1.1	1.02	M 4
HAWKI.2014-01-19T07_49_48.826.fits	J	2	0.74	1.44	NGC 4157

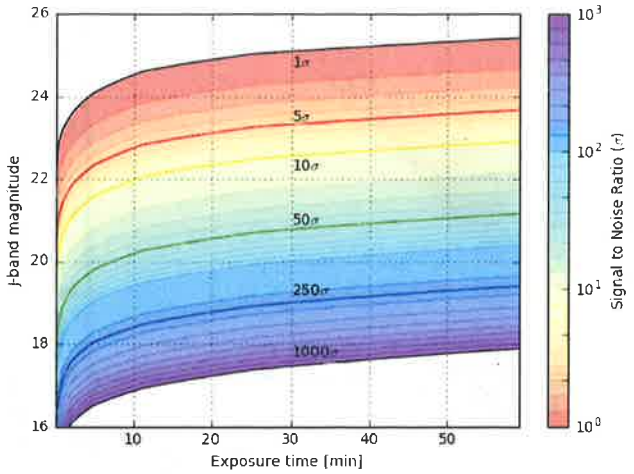

Fig. 4. A grid of hundred stars were observed for different durations between 1 and 60 minutes using SimCADO configured to model the UT4/HAWK-I optical system. The 5σ contour in this graph is $\sim 0.5^{m}$ lower than the theoretical 5σ detection limits as returned by the ESO HAWKI ETC. However the one hour 5σ magnitude limit ($J = 23.7^{m}$) is within 0.2^{m} of the limit published by Kissler-Patig et al. (2008).

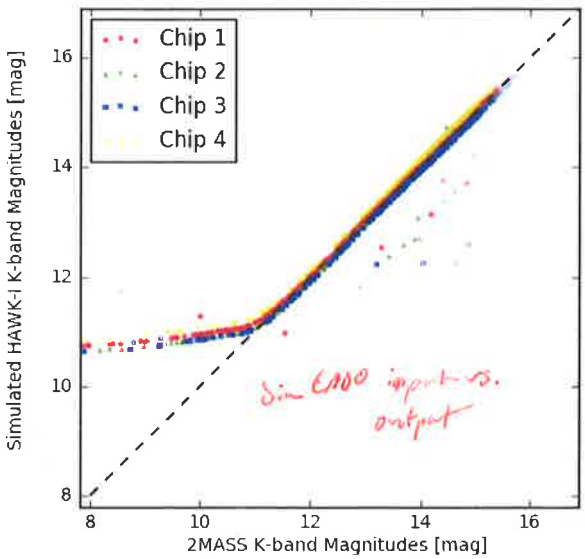

Fig. 5. Instrumental K-band magnitudes from image of M 4 simulated with SimCADO versus the 2MASS catalogue K-band magnitude. The zero-point used was 27.2^{m} . The one-to-one correlation was to be expected because the description of M 4 used by SimCADO to generate the images was based on the 2MASS catalogue. The deviations from the one-to-one line show where the photometry pipeline we used broke down. The cloud of points below the line shows where two stars were close enough together that the pipeline chose the wrong star. It was set up to choose the brightest star within a 1″ radius each set of coordinates OC: ???. Secondly, the deviation from the one-to-one line around $K_s = 11^{m}$ is due to the fixed aperture used in the photometry pipeline. The wings of the HAWK-I PSF meant that the flux from stars brighter than $K_s = 11^{m}$ leaked into the background aperture. Consequently an incorrectly high background flux was subtracted from the star, artificially lowering its measured magnitude. The effect of the different gain values for the HAWK-I detector chips is also visible as the slight offset between the different coloured dots.

ent magnitudes of all sources in the respective HAWK-I fields of view. These `source`-objects were fed into the SimCADO model of HAWK-I and the `Detector` module was read-out. The resulting images were analogues of the raw images generated by the HAWK-I detector chips. They contained raw pixel counts in ADUs. We used aperture photometry to determine the total flux of each star and then compared flux values to the theoretical fluxes calculated from the 2MASS magnitudes. The SimCADO fluxes are in excellent agreement with the 2MASS fluxes. This was to be expected as the 2MASS catalogue provided the input for the SimCADO source model. Although Fig. 5 shows a dependent correlation (OC: ???) between the two axes, we have included this figure to show the reliability of SimCADO when propagating flux through the model of the optical train. The deviation from the one-to-one line in Fig. 5 is due to a combination of two factors: SimCADO recreating the non-linearity of the HAWAII-2RG detectors for pixel counts higher than $\sim 100,000$, as well as the background annulus used in the aperture photometry being too small for the brightest stars. While an adjustable size for the annulus would have slightly improved the comparison, it was not deemed necessary to illustrate SimCADO's ability to accurately propagate flux through the optical train.

The same aperture photometry method was also applied to the raw HAWK-I images from the archive. Fig. 6 shows a comparison between the total aperture flux for stars in a real K-band image of M 4 and its simulated counterpart. There is a good correlation between the fluxes extracted from the two images. For chips 1 and 2 more than 75 % of stars with A-grade 2MASS photometry fall within these bands. For chips 3 and 4 it is more than 85 %. Approximately 55 % of the sources with C-grade or less photometry flags fell outside the ±30 % bands. When investigating these sources we found a large fraction to be single entries in the 2MASS catalogue which were resolved out into two stars in the HAWK-I images. In these cases our photometric pipeline selected the brightest of the resolved stars in the HAWK-I images and measured its flux. The flux of the star in SimCADO was based on the 2MASS catalogue, which includes the flux from all the unresolved stars, and was thus brighter in the simulated images. This is the primary cause of the scatter seen above the one-to-one line in Fig. 6. As the artificial globular cluster for SimCADO is based on the 2MASS catalogue for M 4, there are no sources fainter than the 2MASS detection limit. The presence

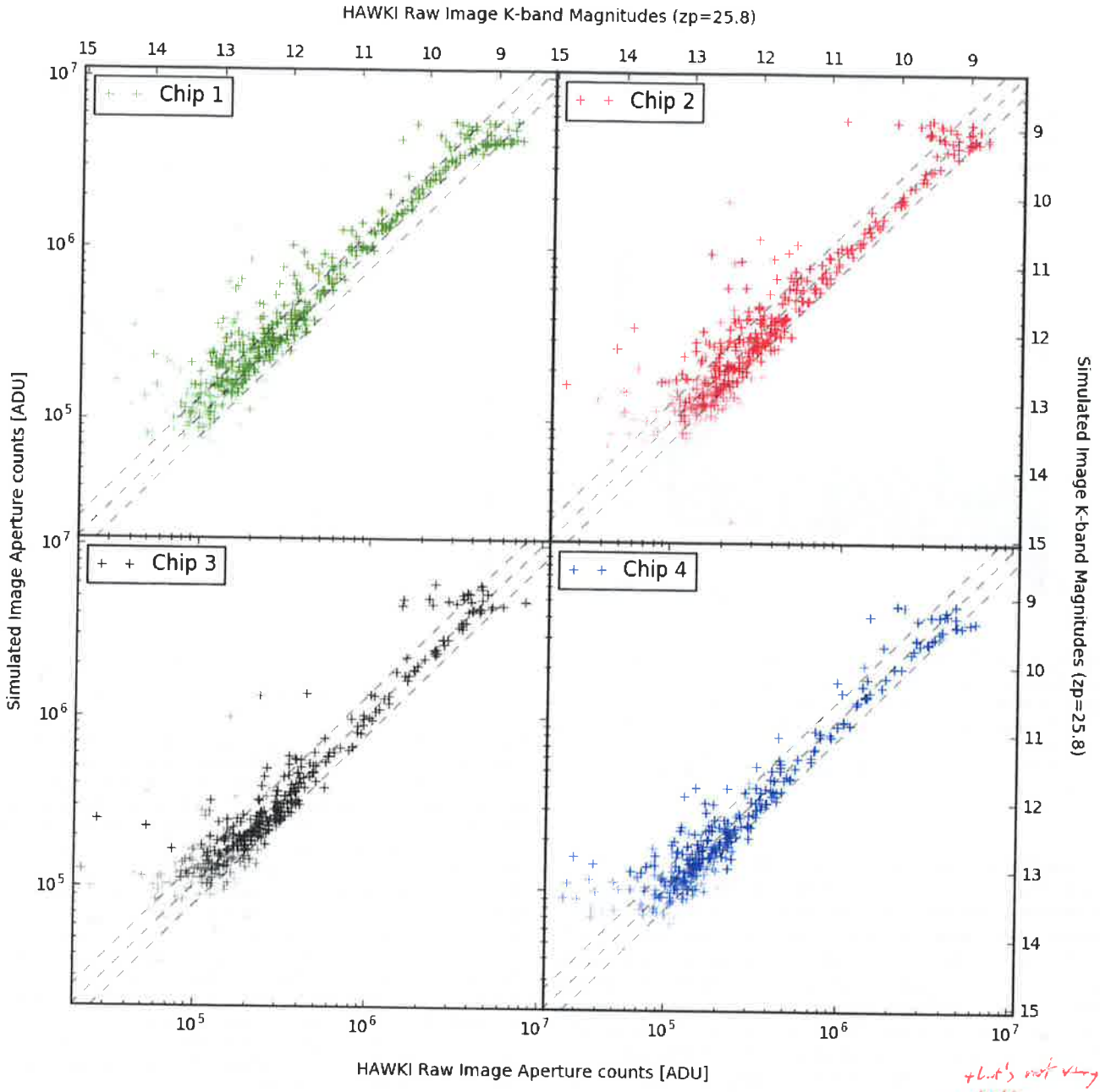

Fig. 6. Flux counts from aperture photometry of the stars in the simulated and real Ks-band images of M 4. Each of the detector chips is plotted here as they each covered a different region of M 4 and each chip has a different gain factor. The strength of the symbols is determined by the photometric quality flag in the 2MASS catalogue. The dashed lines are the $\pm 0.3^{m}$, or 30 % flux difference intervals. For chips 1 and 2 more than 75 % of stars with A-grade 2MASS photometry fall within these bands. For chips 3 and 4 this is > 85 %. Approximately 55 % of the sources with C-grade or worse 2MASS photometry flags fell outside the ±30 % bands. When investigating these sources we found a large fraction to be single entries in the 2MASS catalogue, but were resolved out into two (or more) stars in the HAWK-I images.

of the fainter background sources, and thus a non-uniform increase in the background flux in the real images further reduced the accuracy of the photometric measurements for sources with magnitudes $K_s > 12^{m}$. In this faint regime "hot" or "dead" pixels also affect the accuracy of the photometry. As we did not provide SimCADO with a pixel map for HAWK-I, malfunctioning pixels included in the simulated images were not the same as those on the HAWK-I detectors. These pixels are the primary cause of the scatter below the one-to-one line in Fig. 6. Finally, the small but uniform $< 0.1^{m}$ shift in the photometry between detector chips was caused by the difference in the detector gain factors (Kissler-Patig et al. 2008).

Aside from reproducing the photometric characteristics of stars on the detector plane, (OC: ???) and more important for making predictions for MICADO and the ELT, is SimCADO's ability to accurately reproduce the background flux distribution.

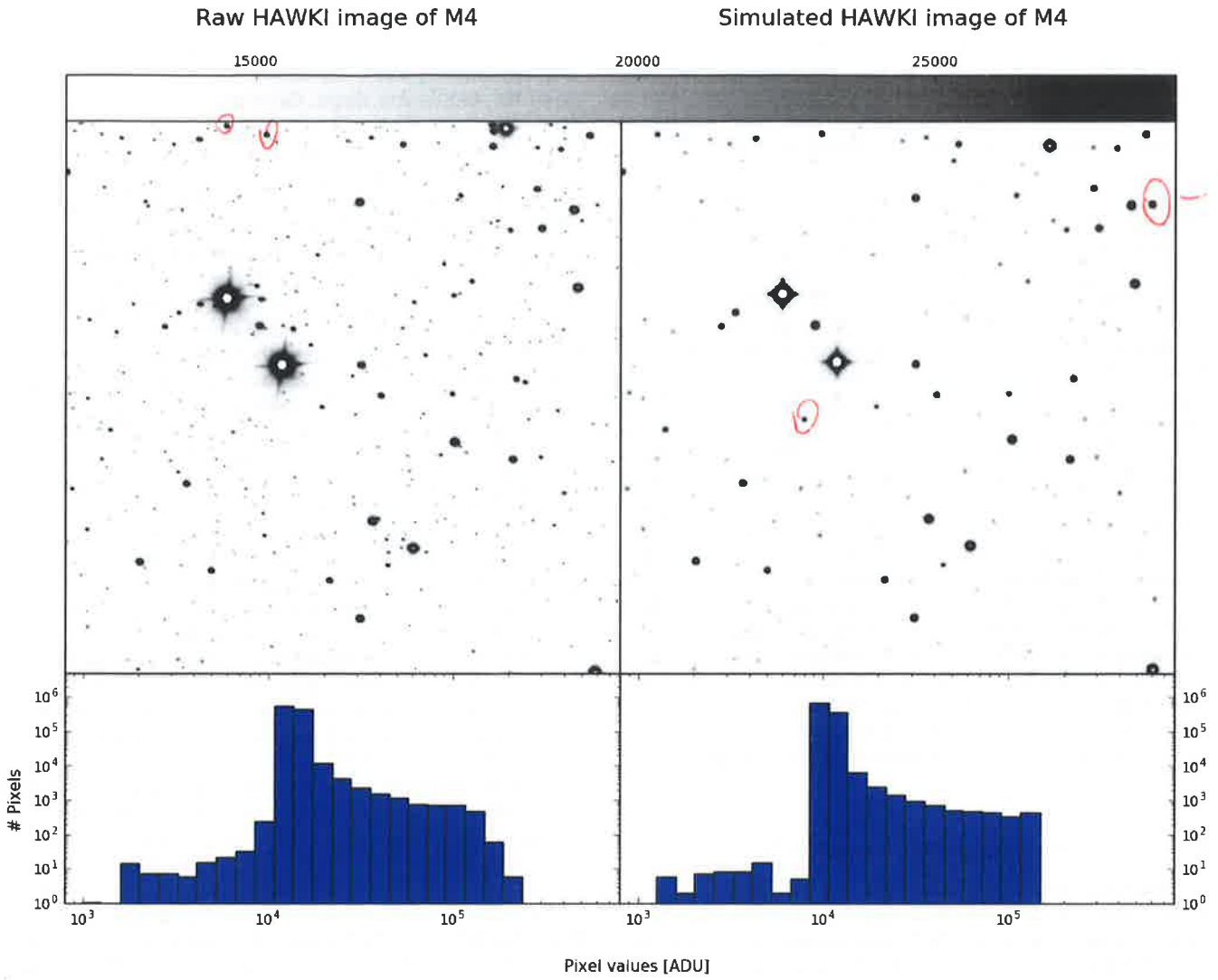

Fig. 7. Top: A comparison of a raw HAWK-I image (left) with a simulated image (right) from SimCADO for the same field near M 4. Features created by the optical train (e.g. diffraction spikes) and by the detector (e.g. saturation) can be seen in both the real and simulated images. The apparent size of the PSF for the brightest stars in the simulated images is smaller than in the real images because SimCADO does not currently model leakage from saturated pixels into neighbouring pixels. The simulated images were based on the 2MASS catalogue. As such no sources fainter than the 2MASS detection limit were simulated. Bottom: The distribution of pixel counts for the real (left) and simulated (right) images is given here to illustrate that SimCADO is capable of recreating observations with no "real world" input. The discrepancy in the shape of the histogram for pixel counts less that 10 000 is due to the low resolution custom made linearity curve used by SimCADO. Because of this the saturated pixels in the brightest stars are not modelled correctly in SimCADO. However, as such pixels are often flagged as unusable by reduction pipelines, refining the accuracy of the linearity curve for SimCADO was deemed less than critical.

As there was no information readily available for the strength of the sky background for the raw archive images, we assumed standard sky background magnitudes as given by Cuby et al. (2000). This assumption was adequate for SimCADO to reproduce the shape of the flux histogram as shown in Fig. 7. It should be noted that the sky background varied between the three sets of archival data. This resulted in background fluxes from SimCADO being $\sim 0.1^{m}$ lower than the backgrounds in the raw J and Ks images from the 2007 observations of M 4. For the 2015 Ks-band observation the simulated image had a background flux on the order of $\sim 0.4^{m}$ fainter than in the raw HAWK-I image. Given that Moreels et al. (2008) report that NIR sky backgrounds can vary up to 0.75^{m} per night, we concluded that this difference was due to the observational conditions[11]. Further work is currently being done to implement an extended background model so that SimCADO is able to also reliably reproduce the sky background for various combinations of observing conditions such as airmass, seeing and precipitable water vapour.

5. Predictions for MICADO's point source sensitivity

MICADO will offer diffraction-limited imaging with a PSF width of ~ 7 and ~ 12 milli-arcseconds in the J and Ks filters respectively. This will allow stars in densely populated regions such as the centres of globular clusters to be easily resolved (see

[11] https://www.eso.org/sci/observing/phase2/ObsConditions.html

Fig. 10). Indeed the majority of the primary science cases for MICADO revolve around accurately resolving points sources. Thus it is important to know the sensitivity limits of the imaging mode well in advance of MICADO going on-sky. Here we briefly present the results of a series of SimCADO simulations aimed at determining the observational limits for MICADO. The model of the optical train used for these simulations was the default MICADO wide-field imaging mode, as described in Sect. 2. The method for measuring the signal-to-noise ratio was identical to the method used for the HAWK-I verification run described in Sect. 4, except the minimum integration time was extended to 2.6 seconds. This reflects the read-out time of the HAWAII-4RG detectors. Also the grid of stars used for the test observations included only stars with magnitudes between 16 and 32 as the extended diffraction spikes from brighter stars negatively affected the photometry of the nearby fainter stars. The extent to which such PSF artefacts influence the accuracy of both the photometry as well as the completeness of observed stellar populations is indeed an important question and will be addressed in a companion paper. For this study, however, we simply removed the stars whose PSF artefacts contaminated their neighbours' apertures.

It should be noted that the PSFs for these simulations were produced by the SCAO working group for the MICADO consortium (Vidal et al., 2017) **(OC: full reference in bibtex)** specifically for inclusion in the SimCADO package. They were generated using the current state-of-the-art adaptive optics simulations and describe the residual PSF after the AO loop has been closed. The simulations were run for a 14.7^{m} guide star that is 5″ off-axis. The targets were observed at the zenith. The Strehl Ratio of the PSFs were 0.29, 0.51 and 0.68 for the J, H and Ks band respectively.

5.1. Point source sensitivity vs. exposure time

For studies of stellar populations, the detection limit is often set to 5σ, where σ is the level of total background noise. However, in order to achieve a high level of astrometric precision (e.g. down to levels of $\sim$ 1/30th of a pixel, or $\sim$ 50 µas), a much higher signal-to-noise ratio is required, e.g. $\sim 250\sigma$. Table 4 lists MICADO's limiting magnitudes for the photometric and astrometric cases. For an exposure time of 5 hours, we find the limiting magnitudes (Vega) for a 5σ detection to be 28.7^{m}, 27.9^{m} and 27.3^{m} in the J, H and Ks broadband filters respectively. For the narrow-band filter Brγ we find a limiting magnitude of 26.0^{m}. The J and H limiting magnitudes match those from the ELT exposure time calculator[12] to within 0.1^{m}. The Ks estimate is 0.2^{m} weaker than that from the ETC.

For astrometric purposes, we find the limiting magnitudes to be 24.2^{m}, 23.5^{m}, 22.9^{m} in J, H and Ks filters and 21.7^{m} in the Brγ filter. All magnitudes are given in the Vega system.[13] Fig. 8 is an expanded graphical representation of Table 4 that shows the full range of limiting magnitudes for observations from the shortest integration time to a full 10 hour observing program and for signal-to-noise ratios of 1σ to 1000σ.

5.2. Point source saturation limits

Given the ELT's collecting area of 978 m^2, it is also important when determining observational strategies to know the saturation limits of the detectors. Basic aperture photometry is only reliable when the maximum pixel values inside the aperture are below the saturation threshold. Advanced techniques such as PSF fitting will naturally allow this threshold to be extended. However, given the unorthodox shape, the many sharp artefacts, and the dynamic nature of an AO corrected PSF, the use of advanced photometric methods will prove challenging. Therefore in order to set conservative limits on the accuracy of photometry for bright sources with MICADO we decided to define photometric reliability as stars with only unsaturated pixels.

The minimum read-out time for a full H4RG detector will be 2.6 seconds. MICADO will also offer a fast readout mode for windowed regions of the detector capable of reading out e.g. a 100 × 100 pixel area at a rate of 200 Hz (DIT $\sim$ 5 ms). To calculate the bright star limits we took the brightest star from the simulated images that had no values over the correctable non-linear regime. As there is little data publicly available for the performance of HAWAII-4RG detectors, we assumed the characteristics will be similar to the HAWAII-2RG chips. According to Loose et al. (2007), all detectors in the HAWAII-RG family have a correctable linearity regime (within 5 %) of $\sim 10^{5}$ e^{-}/pixel with a full well depth of $< 1.5 \cdot 10^{5}$ e^{-}/pixel. Table 5 shows the brightest magnitudes that can be observed in the J, H, Ks and Brγ filters without any pixels saturating.

As a sanity check, we compared the limits in Table 5 to the saturation limits given by the ELT exposure time calculator. The ETC uses a slightly different configuration for the imaging mode, the most notable differences being a collecting area of 1100 m^2 and a plate scale of 5 mas. After normalising the results from the ETC, we find that SimCADO matches the ETC's calculations to within 0.1^{m}.

It is worth noting that in the standard wide-field imaging mode with an integration time of 2.6 s, MICADO will saturate around the detection limit of the 2MASS survey, i.e. $J = 15.8^{m}$, $H = 15.1^{m}$ and $K_s = 14.3^{m}$ (Skrutskie et al. 2006). On the one hand, this is a testament to the extreme increase in observing capabilities that the ELT and MICADO will provide. On the other hand, this will prove problematic for observers as all observations within $\sim 1'$ **(OC: arcmin or arcsec?)** of a 2MASS source will need to account for the effects of overly bright sources. Given that the diffraction spikes of the ELT's PSF are long and prominent, there is a good chance that they will cause issues with the reduction and analysis of fainter, more interesting regions.

5.3. Extended Source sensitivities

(KL: Will we do a more detailed investigation for extended sources here ???)

(KL: List background fluxes for each filter and work backwards to get the 5σ sensitivity for a given exposure time - easy right?)

(KL: Needs to be completed still)

With the ELT's 978 m^2 collecting area and the diffraction limited performance afforded by both MCAO and SCAO modes, MICADO will have an unprecedented ability to observe faint point sources. Extended sources will not see the same level of improvement. To a good approximation, the flux per resolution element from a point source scales linearly with collecting area, irrespective of the size of the resolution element. For extended sources however, flux scales inversely with the angular area of the resolution element.

A quick comparison with the values of the NIR arm of the WFC3 instrument (Rajan & et al. 2011) on the Hubble Space Telescope (HST) shows that MICADO will be a factor of almost five times less efficient than WFC3 when it comes to collecting

[12] https://www.eso.org/observing/etc/bin/simu/elt_ima

[13] To convert to the AB system $\sim$ 0.9, $\sim$ 1.4 and $\sim$ 1.85 should be added to the J, H and Ks magnitudes respectively.

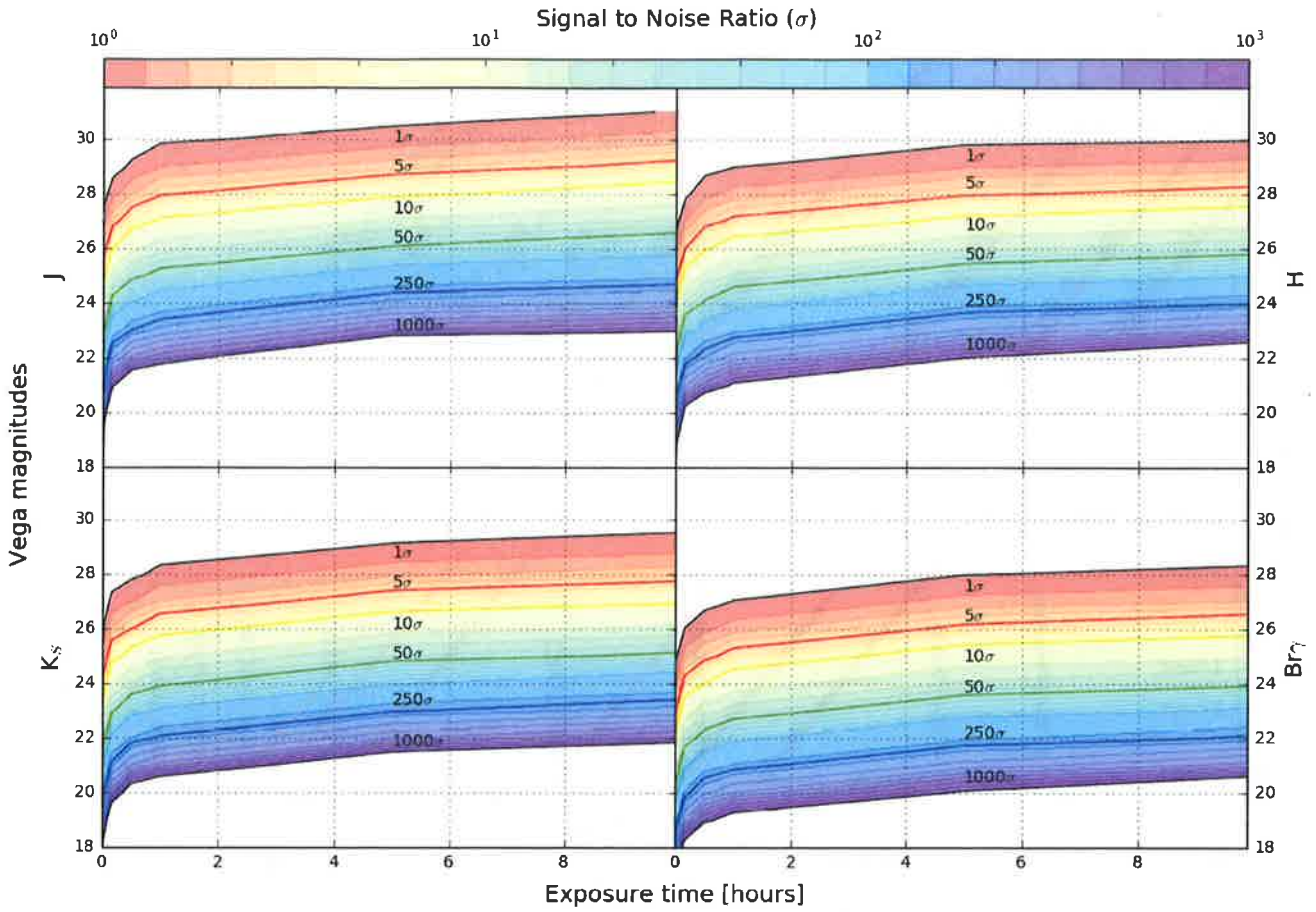

Fig. 8. Limiting magnitude plots for the wide field (4 mas/pixel) imaging mode of MICADO at the ELT in Vega magnitudes. Signal-to-noise ratios above 5σ are sufficient for photometry. High precision astrometry requires stronger detections $\sim 250\sigma$. It should be noted that these magnitudes apply to the current design of MICADO and the ELT. At the time of publication MICADO is still in its preliminary design phase. As such we expect small changes in these values as the MICADO design matures.

Table 4. Specific point-source sensitivities for the NIR broadband filters J, H and Ks and the narrow band filter Brγ . 5σ and 10σ are generally accepted detection limits for photometric measurements, while for accurate astrometry signal-to-noise ratios above 250σ are required. The errors on these magnitudes are $\pm 0.1^{m}$. It should be noted that these magnitudes apply to the current design of MICADO and the ELT. At the time of publication MICADO is still in its preliminary design phase. As such we expect small changes in these values as the MICADO design matures.

Filter	SNR	2.6 sec	10 sec	1 min	10 min	1 hr	5 hrs	10 hrs
J	5σ	23.4^{m}	24.4^{m}	25.6^{m}	26.7^{m}	27.8^{m}	28.7^{m}	29.0^{m}
	10σ	22.6^{m}	23.6^{m}	24.8^{m}	26.0^{m}	27.0^{m}	27.9^{m}	28.2^{m}
	250σ	18.7^{m}	19.9^{m}	21.1^{m}	22.4^{m}	23.4^{m}	24.2^{m}	24.6^{m}
H	5σ	23.0^{m}	23.8^{m}	24.8^{m}	26.0^{m}	27.0^{m}	27.9^{m}	28.3^{m}
	10σ	22.2^{m}	23.0^{m}	24.0^{m}	25.3^{m}	26.2^{m}	27.1^{m}	27.5^{m}
	250σ	18.6^{m}	19.4^{m}	20.4^{m}	21.7^{m}	22.7^{m}	23.5^{m}	23.9^{m}
Ks	5σ	22.4^{m}	23.1^{m}	24.1^{m}	25.6^{m}	26.4^{m}	27.3^{m}	27.7^{m}
	10σ	21.6^{m}	22.4^{m}	23.4^{m}	24.8^{m}	25.6^{m}	26.5^{m}	26.9^{m}
	250σ	18.0^{m}	18.9^{m}	19.8^{m}	21.0^{m}	22.1^{m}	22.9^{m}	23.3^{m}
Brγ	5σ	20.6^{m}	21.8^{m}	22.9^{m}	24.1^{m}	25.2^{m}	26.0^{m}	26.3^{m}
	10σ	19.8^{m}	21.0^{m}	22.1^{m}	23.4^{m}	24.4^{m}	25.2^{m}	25.6^{m}
	250σ	16.0^{m}	17.1^{m}	18.4^{m}	19.8^{m}	20.8^{m}	21.7^{m}	22.1^{m}

light from extended sources. However, MICADO will provide a vast improvement in our ability to resolve structures on scales $\sim 32\times$ smaller than WFC3-IR on HST. For example, at a redshift of $z = 2$ where the proper angular transverse distance is at its smallest ($\sim 8.5\,\mathrm{kpc\,arcsec^{-1}}$), MICADO should be able to resolve structures on scales of 30 pc. This is to be compared to scales of 300 pc and 1 kpc with JWST and HST, respectively.

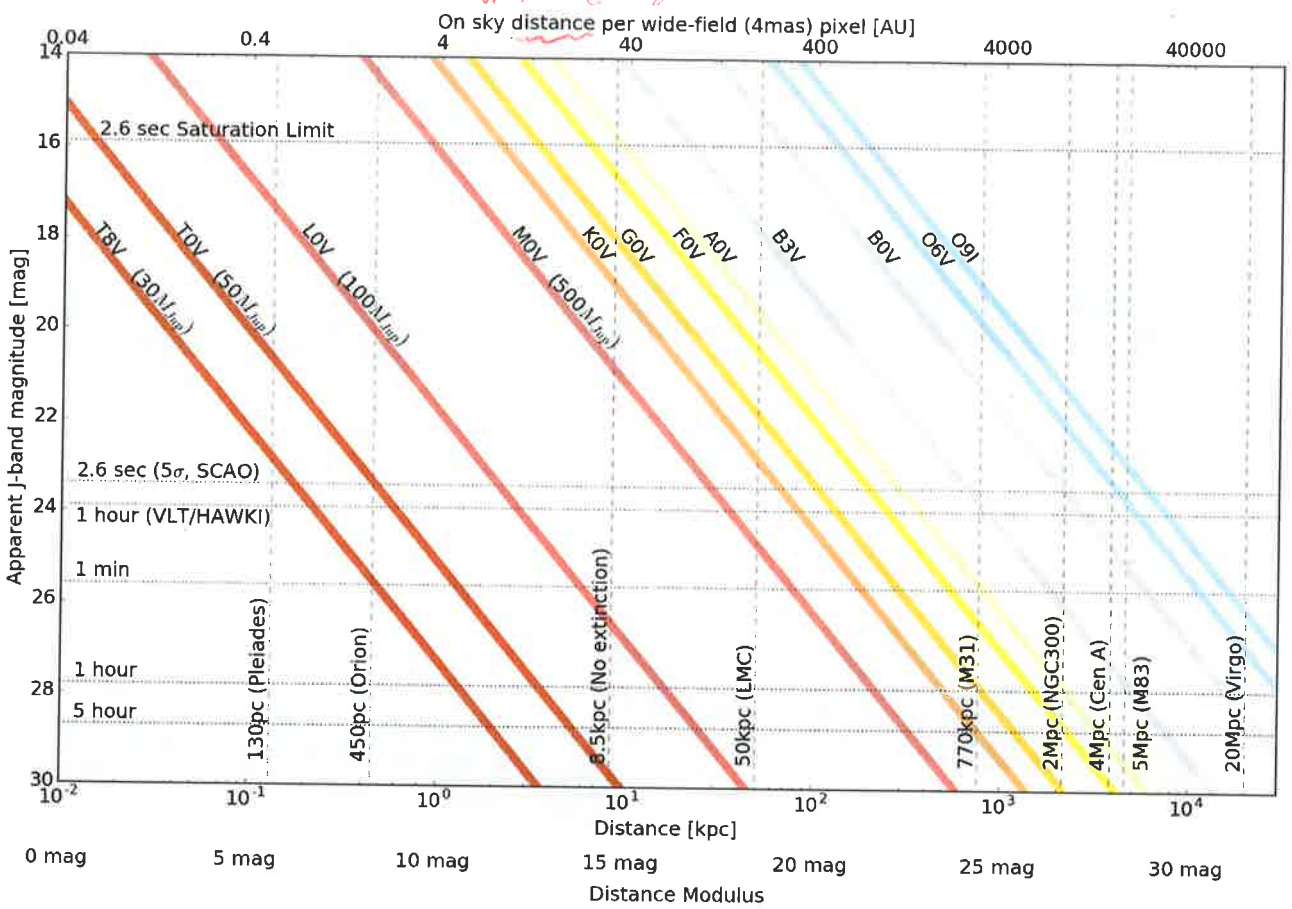

Fig. 9. The coloured lines represent the apparent magnitude of the major spectral types with increasing distance. The dashed horizontal lines, unless otherwise stated, represent the 5σ detection limits for various exposure times with MICADO. When a coloured line crosses below a horizontal line, it means that this type of main-sequence star will no longer be detectable by MICADO at the distance where the cross occurs. As a reference, the dashed vertical lines show distances to well known astronomical objects. It is worth noting that what HAWK-I can do in 1 hour, MICADO can do in 2.6 seconds. While this comparison may seem ludicrous, the ELT has a primary mirror ~ 20× larger that of UT4 at the VLT and the smaller plate scale of MICADO means a factor of ~ 35× less background flux per pixel.

5.4. Spectral type with distance

Four of the major science drivers for MICADO rely on determining the properties of stellar populations. Hence we found it prudent to use the sensitivity estimates from SimCADO to calculate limiting distances for a 5σ detection for different spectral types. Fig. 9 shows the apparent magnitude of a selection of main-sequence stars with increasing distance as well as the sensitivity limits for MICADO for a range of exposure times. We used the main sequence absolute magnitudes given in Table 5 of Pecaut & Mamajek (2013).[14] As the brightest stars in the main sequence cover almost the same magnitude range as all giant and most supergiant stars, those readers interested in the limiting distances for stars that have left the main sequence are requested to use the distances for a main sequence star with an equivalent absolute magnitude. Using SimCADO we have determined that MICADO should be able to detect all A-type stars in Centaurus A at a distance of 4 Mpc with a 5 hour observation. A 1 hour observation should be sufficient to detect all stars down to the Hydrogen burning limit ($M < 0.08 M_{\odot}$) in the Magellanic Clouds (~ 50 kpc). However, it is worth mentioning that at this distance all stars brighter than B1V will saturate within the shortest exposure time (DIT = 2.6 s). For more case specific distance limits based on the SimCADO limiting magnitudes, we direct the reader to Fig. 9. The equivalent plot for the Ks filter is included in the Appendix. These distance estimates are based on an ideal case scenario and the current design of the MICADO optical train. Therefore Fig. 9 should be understood as illustrating upper limits for the distance estimates. For example, we have assumed no extinction along the line of sight. Nor have we taken into account the increased background levels in crowded field. Both effects will undoubtedly reduce the distance estimated by varying amounts. To what degree the level of crowding affects these distance estimates will be the focus of a companion paper.

[14] Additional information for the L and T dwarves (not reported by Pecaut & Mamajek 2013) were taken from the associated website `http://www.pas.rochester.edu/~emamajek/EEM_dwarf_UBVIJHK_colors_Teff.txt`

6. Discussion, open issues and assumptions

6.1. Discussion on the differences between the simulated and the real HAWK-I images

Overall the simulated images of M 4 and NGC 4147 compared favourably with the raw observations from the ESO archive.

Table 5. Saturation Limits for MICADO assuming an effective detector well depth of 10^5 e^-/pixel. The shortest integration time for a full detector will be ~ 2.6 s, while a faster readout mode will be available for smaller windowed regions (Davies et al. 2010). Given the current detector specifications a 100×100 pixel window might achieve a read-out frequency of 200 Hz, or 5 ms per exposure. The limits are split between the two default imaging modes of MICADO: Wide-field mode (4 mas/pixel, ~ 50″ FoV), and the zoom mode (1.5 mas/pixel, ~ 20″ FoV). While the ESO exposure time calculator for the ELT has a slightly different configuration for the imaging mode, when the results are normalised we find that the SimCADO saturation limits are within 0.1^m of the ETC's limits.

Filter	DIT	4 mas/pixel	1.5 mas/pixel
J	2.6 s	15.9^m	13.6^m
	0.005 s	14.0^m	11.8^m
H	2.6 s	15.6^m	13.4^m
	0.005 s	13.8^m	11.6^m
K_s	2.6 s	14.8^m	12.5^m
	0.005 s	13.0^m	10.8^m
Brγ	2.6 s	12.0^m	9.9^m
	0.005 s	10.2^m	8.1^m

The distribution of pixel flux, background level and noise, total star fluxes and positions, detector noise and saturation, were well reproduced in the simulated images. Magnitudes derived from aperture photometry on the simulated images matched almost perfectly with the 2MASS catalogue for all stars with $J, Ks > 11^m$. When comparing photometry between the simulated and archive images, around two thirds of all the stars measured had flux differences between the images within $\pm 0.3^m$. The scatter seen in Fig. 6 is a combination of unresolved sources in the 2MASS catalogue being resolved by HAWK-I, and SimCADO not including the hot pixels on the HAWK-I detectors. Hence this scatter shows that there is a need for a better description of the globular clusters. An extrapolation of the source catalogue down to the detection limit of HAWK-I would be desirable. However, as the coordinates of the fainter sources are unknown, this would likely cause the scatter to increase rather than decrease. With the ELT's ability to detect sources down to $J \approx 29^m$, the prevalence of background sources in this regime will indeed need to be addressed and simulated accurately.

The level of background flux generated by SimCADO for the J and Ks filters is in line with the flux levels returned by the ESO exposure time calculator for HAWK-I. However, only archive J and Ks images from 2007 had background levels as low as the ETC and SimCADO. The other two J and Ks images had levels 10 % and 30 % higher. While there is an abundance of information on the weather conditions during the observations, we were unable to find estimates for the measured sky background. We therefore used the standard Paranal background magnitudes for the simulations. As NIR sky background levels can vary by up to 0.75^m over the course of a night (Moreels et al. 2008), we do not see the difference between the simulated and real background fluxes in these images as a major failure of the software. Moreover, sky dynamic background variation is yet another effect that should be added to a future release of SimCADO.

A final caveat for the software verification is that the model of the optical train for UT4/HAWK-I is based on the information available on the ESO website and from the HAWK-I user manual. Despite our due diligence it is possible that some of the data used by SimCADO is inaccurate or not up to date. In order to further test how SimCADO reacts to different sets of observing conditions (airmass, seeing, etc), we submitted a ESO proposal in Period 100 for technical time on HAWK-I. We are waiting on the completion of the observing run before embarking on a new validation campaign. This should allow us to further increase the accuracy of the simulated images by allowing us to implement each aspect of the atmospheric background separately.

6.2. Accuracy of the SimCADO sensitivity predictions

SimCADO was verified by comparing simulated images with real HAWK-I observation. Furthermore, estimates from SimCADO images of the detection and saturation limits for observations with MICADO fall within 0.1^m of the values given by the ELT exposure time calculator (after normalising the two optical train configurations). These two results give us confidence that the predictions of MICADO's sensitivity can be accurately determined from simulations with SimCADO. These simulations have however been conducted using several simplifications. For example, the atmospheric conditions were assumed to mirror those of the average night at Paranal. Given that the NIR sky background can vary up to ~ 0.2^m within 15 minutes (Moreels et al. 2008) and that it is also dependent on the level of water in the air as well as the airmass of the pointing, it is clear that the true detection limits of MICADO will vary from this first round of predictions with SimCADO. Furthermore, the PSF used for the current round of SimCADO predictions was uniform across the field of view. This will definitely not be the case. Reductions in the Strehl ratio of > 50 % over the MICADO field of view are expected for SCAO observations (Clénet et al. 2015). Such variations will have a marked impact on sensitivity in the outer regions of the MICADO focal plane.

Another challenge for estimating the performance of the telescope and instrument will be the ELT's PSF. Accurate photometry of bright sources, extracting faint sources that are covered by the wings of the brighter sources, and accurate astrometry all rely on accurate knowledge of the shape of the PSF. As can be seen in Fig. 10, the discrete nature of the diffraction spikes of the SCAO PSF could easily confuse a star finding algorithm. Additionally, the PSF will rotate with respect to the field over the course of an observing run due to the ELT's alt-azimuth mount. This would greatly complicate the standard stack and subtract technique for data reduction. Arguably though, this may prove advantageous as it would provide a natural rotational dithering, which may smooth out the sharp features of the PSF. An alternative approach would be to deconvolve the images with a spatially varying model of the PSF. This would however require multiple descriptions of the PSF for each detector frame, which could slowly become a challenging data management task. Whether this task belongs in the automated data pipeline or is left to the user is still undecided. A different approach would be to use a blind deconvolution algorithm (Vorontsov & Jefferies 2017). Recent results are encouraging, although it remains to be seen how well this approach works for spatially varying PSFs. In any case, the complex PSF of the ELT will present a challenge to standard data analysis techniques. How the PSF artefacts of bright stars affect the surrounding environment is a question that should be considered in the earliest stages of planning observations with the ELT and MICADO.

6.3. Future functionality for SimCADO

The results of the first verification run show that SimCADO is capable of recreating observations with only descriptions of the optical elements as input. There are, however, still several as-

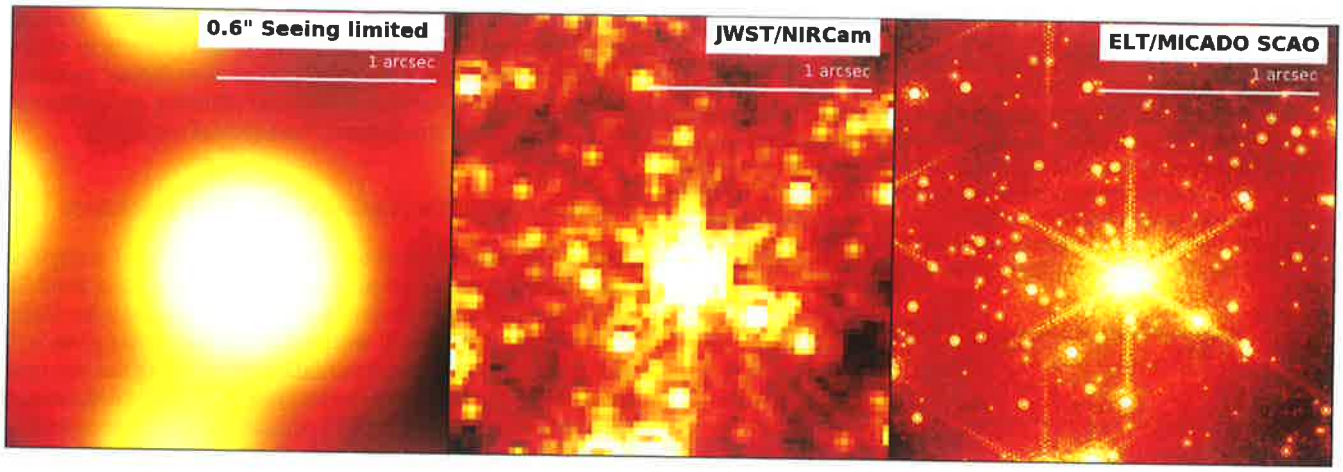

Fig. 10. An illustration of the improvement that MICADO's increase in resolution **(OC: missing word/s?)** when resolving the members of densely populated regions. Left: A dense stellar field observed with 0.6 arcsecond seeing. Middle: The same field as will be observed by NIRCam on JWST. Right: A prediction of how the dense stellar field will look when observed by MICADO in wide-field mode (4 mas/pixel).

pects that require attention by the development team. In short they are:

Atmospheric variations: SimCADO uses a standardised spectrum for the sky background, scaled to the required background level, to provide the background flux for any chosen filter. Currently this atmospheric spectrum is independent of the observational setup, i.e. it does not change as airmass or PWV conditions change. For the verification run described here, these points were not relevant: the archival data for M 4 were taken close to zenith and the image of NGC 4147 (airmass ~ 1.44) was primarily used as a control for its different exposure length. Functionality to accurately model the effects of different observational conditions are in development and will be included in a future release of the software.

PSF variability: While not as important for a seeing-limited instrument, the variations in the shape of the PSF over the field of view for observations conducted with adaptive optics is not a trivial effect. The development team is currently in the process of implementing functionality to include the off-axis PSFs provided by the SCAO and MCAO simulation teams. Furthermore the PSF is based on the post-AO PSF delivered by the AO simulation teams. The exposure times are assumed to be long enough that the PSF should not vary noticeably between exposures. Whether or not this assumption holds for all time scales remains to be investigated.

Distortion effects: For photometric studies optical distortions are a nuisance. For astrometric studies they are critical. SimCADO includes the functionality to shift point sources on the sub-pixel level. As such we are currently investigating the best way to implement the use of distortion maps in the model of the optical train.

Spectroscopy: MICADO will also include the optics to function as a long slit spectrograph. Development is ongoing with the implementation of this mode into SimCADO.

Non-common path aberrations: Only the effective loss in flux due to NCPAs is currently included in SimCADO. This is a function of wavelength and as such can be modelled effectively as an additional transmission curve. The spatial aspects of the NCPAs in the context of the MICADO optical train need to be investigated further before we can implement them into SimCADO.

Although there is still much work to do, SimCADO is already capable of simulating raw detector read-outs for each of the MICADO imaging modes. This alone covers the majority of the primary science drivers for MICADO. It should also be noted that MICADO is still in the preliminary design phase and so the composition of the optical train, and therefore the default data installed alongside SimCADO, are likely to change in the future. However, we foresee no radical changes to the design, and thus no radical changes to the sensitivity estimates we have presented in this paper.

7. Summary

As part of the design activities for the MICADO instrument we have developed an instrument data simulator in Python: SimCADO. The software is capable of generating detector frames for any given optical train configuration and source object description. A summary of our activities and results is as follows:

- In conjunction with the MICADO instrument team we have developed a modular python package that allows us to model each element in the optical train separately. The software allows the user to fully control the configuration of the optical train as well as the description of the astronomical object to be observed. Images produced by the package are in the standard FITS format and can be treated as coming directly from a telescope.
- We configured SimCADO to mimic the UT4/HAWK-I optical train and "observed" two globular clusters with this setup. A comparison to archive data for the same globular clusters showed that SimCADO is capable of reproducing all the major and most of the minor effects that are seen in raw detector frames from HAWK-I. A photometric comparison shows a one-to-one correlation between the flux observed in the archive and simulated images. Although there is scatter around this line, the primary source of uncertainty lies with the photometric analysis of the archive data and not with the

simulated images. Additionally SimCADO is able to reproduce the detection limits given by the ESO exposure time calculator for a 1-hour observation with HAWK-I.

- Using the configuration for the ELT/MICADO optical train we simulated a grid of stars to find the detection limits for different exposure times. We have shown that the 5 hour detection limits in Vega magnitudes are: $J = 28.7^{m}$, $H = 27.9^{m}$ and $K_s = 27.3^{m}$, while the saturation limit for the shortest exposure time (MINDIT = 2.6 s) in the wide-field (4 mas/pixel) mode are similar to the 2MASS detection limits: $J = 15.9^{m}$, $H = 15.6^{m}$ and $K_s = 14.8^{m}$. The use of the zoom mode (1.5 mas/pixel) in conjunction with a narrow band filter, such as the Br γ filter, would reduce increase this limit to $\sim 9.9^{m}$.
- With these detection limits we have shown that MICADO will be capable of detecting individual A0 V stars at a distance of 4 Mpc (Centaurus A), while any star brighter than B1 V at a distance of 50 kpc (LMC) will saturate during the a single minimum length exposure.
- We will be adding the following functionality to SimCADO in the near future: a long slit spectrographic mode, field variable PSFs, variations in atmospheric conditions, as well as further support for the high time resolution and astrometric imaging modes.

We encourage anyone who may want to use the ELT and MICADO for future observations to use SimCADO to simulate their science case in advance. Not only will this help the community to get a feel for what MICADO will be capable of and where possible problems with an observing strategy will be, feedback from users will help us to develop the software in such a way as to meet the needs of the astronomical community.

Acknowledgements. SimCADO incorporates Bernhard Rauscher's HxRG Noise Generator package for python (Rauscher 2015). This research made use of POPPY, an open-source optical propagation Python package originally developed for the James Webb Space Telescope project (Perrin et al. 2015). This research made use of Astropy, a community-developed core Python package for astronomy (Astropy Collaboration et al. 2013; The Astropy Collaboration et al. 2018). This research made use of Photutils (Bradley et al. 2017). This research has made use of "Aladin sky atlas" developed at CDS, Strasbourg Observatory, France (Bonnarel et al. 2000; Boch & Fernique 2014). SimCADO makes use of atmospheric transmission and emission curves generated by ESO's SkyCalc service, which was developed at the University of Innsbruck as part of an Austrian in-kind contribution to ESO. Based on data obtained from the ESO Science Archive Facility under request number Leschinski, #331857. This publication makes use of data products from the Two Micron All Sky Survey, which is a joint project of the University of Massachusetts and the Infrared Processing and Analysis Center/California Institute of Technology, funded by the National Aeronautics and Space Administration and the National Science Foundation (Skrutskie et al. 2006). This research is partially funded by the project IS538003 of the Hochschulraumstrukturmittel (HRSM) provided by the Austrian Government and administered by the University of Vienna. The authors would also like to thank all the members of the consortium for their effort in the MICADO project, and their contributions to the development of this tool.

References

Astropy Collaboration, Robitaille, T. P., Tollerud, E. J., et al. 2013, A&A, 558, A33
Boccas, M., Vucina, T., Araya, C., Vera, E., & Ahhee, C. 2006, Thin Solid Films, 502, 275
Boch, T. & Fernique, P. 2014, in Astronomical Society of the Pacific Conference Series, Vol. 485, Astronomical Data Analysis Software and Systems XXIII, ed. N. Manset & P. Forshay, 277
Bonnarel, F., Fernique, P., Bienaymé, O., et al. 2000, A&AS, 143, 33
Bradley, L., Sipocz, B., Robitaille, T., et al. 2017, astropy/photutils: v0.4
Brandl, B. R., Lenzen, R., Pantin, E., et al. 2008, in Proc. SPIE, Vol. 7014, Ground-based and Airborne Instrumentation for Astronomy II, 70141N
Clénet, Y., Buey, T., Rousset, G., et al. 2016, in Proc. SPIE, Vol. 9909, Society of Photo-Optical Instrumentation Engineers (SPIE) Conference Series, 99090A
Clénet, Y., Gendron, E., Gratadour, D., Rousset, G., & Vidal, F. 2015, A&A, 583, A102
Clenet, Y., Gratadour, D., Gendron, E., Rousset, G., & Sevin, A. 2013, in Proceedings of the Third AO4ELT Conference, ed. S. Esposito & L. Fini, 29
Cuby, J. G., Lidman, C., & Moutou, C. 2000, The Messenger, 101, 2
Davies, R., Ageorges, N., Barl, L., et al. 2010, in Proc. SPIE, Vol. 7735, Ground-based and Airborne Instrumentation for Astronomy III, 77352A
Davies, R., Schubert, J., Hartl, M., et al. 2016, in Proc. SPIE, Vol. 9908, Society of Photo-Optical Instrumentation Engineers (SPIE) Conference Series, 99081Z
Dierickx, P., Enard, D., Merkle, F., Noethe, L., & Wilson, R. N. 1990, in Proc. SPIE, Vol. 1236, Advanced Technology Optical Telescopes IV, ed. L. D. Barr, 138–151
Diolaiti, E. 2010, The Messenger, 140, 28
Diolaiti, E., Ciliegi, P., Abicca, R., et al. 2016, in Proc. SPIE, Vol. 9909, Society of Photo-Optical Instrumentation Engineers (SPIE) Conference Series, 99092D
Finger, G., Dorn, R. J., Eschbaumer, S., et al. 2008, in Proc. SPIE, Vol. 7021, High Energy, Optical, and Infrared Detectors for Astronomy III, 70210P
Gilmozzi, R. & Spyromilio, J. 2007, The Messenger, 127
Jones, A., Noll, S., Kausch, W., Szyszka, C., & Kimeswenger, S. 2013, A&A, 560, A91
Kissler-Patig, M., Pirard, J.-F., Casali, M., et al. 2008, A&A, 491, 941
Leschinski, K., Czoske, O., Köhler, R., et al. 2016, in Proc. SPIE, Vol. 9911, Society of Photo-Optical Instrumentation Engineers (SPIE) Conference Series, 991124
Loose, M., Beletic, J., Garnett, J., & Xu, M. 2007, in Proc. SPIE, Vol. 6690, Focal Plane Arrays for Space Telescopes III, 66900C
Moreels, G., Clairemidi, J., Faivre, M., et al. 2008, Experimental Astronomy, 22, 87
Noll, S., Kausch, W., Barden, M., et al. 2012, A&A, 543, A92
Pecaut, M. J. & Mamajek, E. E. 2013, ApJS, 208, 9
Perrin, M. D., Long, J., Sivaramakrishnan, A., et al. 2015, WebbPSF: James Webb Space Telescope PSF Simulation Tool, Astrophysics Source Code Library
Peterson, J. R., Jernigan, J. G., Kahn, S. M., et al. 2015, ApJS, 218, 14
Posselt, W., Holota, W., Kulinyak, E., et al. 2004, in Proc. SPIE, Vol. 5487, Optical, Infrared, and Millimeter Space Telescopes, ed. J. C. Mather, 688–697
Rajan, A. & et al. 2011, WFC3 Data Handbook v. 2.1 (STSci)
Rauscher, B. J. 2015, PASP, 127, 1144
Schmalzl, E., Meisner, J., Venema, L., et al. 2012, in Proc. SPIE, Vol. 8449, Modeling, Systems Engineering, and Project Management for Astronomy V, 84491P
Skrutskie, M. F., Cutri, R. M., Stiening, R., et al. 2006, AJ, 131, 1163
Stone, R. C. 1996, PASP, 108, 1051
Thatte, N., Tecza, M., Clarke, F., et al. 2010, in Proc. SPIE, Vol. 7735, Ground-based and Airborne Instrumentation for Astronomy III, 77352I
The Astropy Collaboration, Price-Whelan, A. M., Sipőcz, B. M., et al. 2018, ArXiv e-prints [arXiv:1801.02634]
Vorontsov, S. V. & Jefferies, S. M. 2017, Inverse Problems, 33, 055004
Winkler, R., Haynes, D. M., Bellido-Tirado, O., Xu, W., & Haynes, R. 2014, in Proc. SPIE, Vol. 9150, Modeling, Systems Engineering, and Project Management for Astronomy VI, 91500T
Wright, S. A., Walth, G., Do, T., et al. 2016, in Proc. SPIE, Vol. 9909, Society of Photo-Optical Instrumentation Engineers (SPIE) Conference Series, 990905
Zieleniewski, S., Thatte, N., Kendrew, S., et al. 2015, MNRAS, 453, 3754

Appendix A: Distance estimates for main sequence stars in Ks filter

Fig. A.1 shows the Ks-band equivalent of Fig. 9. As described in Fig. 9 the coloured lines represent the apparent magnitude of the major spectral types with increasing distance. The dashed horizontal lines, unless otherwise stated, represent the 5σ detection limits for various exposure times with MICADO. When a coloured line crosses below a horizontal line, it means that this type of main sequence star will no longer be detectable by MICADO at the distance when the cross occurs. As a reference the dashed vertical lines show distances to well known astronomical objects.

Appendix B: Comparison of the HAWK-I and MICADO configuration files

The SimCADO package for Python is in the public domain (**OC: I don't think that's accurate. We need a proper licence!**). We encourage anyone interested in simulating future ELT/MICADO observations to use SimCADO and to report any bugs to the authors. In the interests of transparency and reproducibility, we have included the configuration files that we used to generate SimCADO models of both the HAWK-I and MICADO optical trains. We are also willing to share any of the data files that subsequent users may need in order to reproduce our results. Please contact Kieran Leschinski directly.

Appendix B.1: The MICADO configuration file

The standard configuration file used for the MICADO wide-field (4 mas plate scale) imaging mode.

```
################################################
# Observation Parameters

OBS_DATE                0
OBS_TIME                0
OBS_RA                  90.
OBS_DEC                 -30.
OBS_ALT                 0
OBS_AZ                  0
OBS_ZENITH_DIST         0
OBS_PARALLACTIC_ANGLE   0
OBS_SEEING              0.6

OBS_FIELD_ROTATION      0

OBS_EXPTIME             60
OBS_NDIT                1
OBS_NONDESTRUCT_TRO     2.6
OBS_REMOVE_CONST_BG     no
OBS_READ_MODE           single
OBS_SAVE_ALL_FRAMES     no

OBS_INPUT_SOURCE_PATH   none
OBS_FITS_EXT            0

OBS_OUTPUT_DIR          "./output.fits"


################################################
# Simulation Parameters

SIM_DETECTOR_PIX_SCALE  0.004
SIM_OVERSAMPLING        1
SIM_PIXEL_THRESHOLD     1

SIM_LAM_TC_BIN_WIDTH    0.001
SIM_SPEC_MIN_STEP       1E-4

SIM_FILTER_THRESHOLD    1E-9
SIM_USE_FILTER_LAM      yes
# if "no"
SIM_LAM_MIN             1.9
SIM_LAM_MAX             2.41
SIM_LAM_PSF_BIN_WIDTH   0.1
SIM_ADC_SHIFT_THRESHOLD 1

SIM_PSF_SIZE            1024
SIM_PSF_OVERSAMPLE      no
SIM_VERBOSE             no
SIM_SIM_MESSAGE_LEVEL   3

SIM_OPT_TRAIN_IN_PATH   none
SIM_OPT_TRAIN_OUT_PATH  none
SIM_DETECTOR_IN_PATH    none
SIM_DETECTOR_OUT_PATH   none


################################################
# Atmospheric Parameters

ATMO_USE_ATMO_BG        yes

ATMO_TC                 TC_sky_25.tbl
ATMO_EC                 EC_sky_25.tbl
ATMO_BG_MAGNITUDE       13.6

ATMO_TEMPERATURE        0
ATMO_PRESSURE           750
ATMO_REL_HUMIDITY       60
ATMO_PWV                2.5


################################################
# Telescope Parameters

SCOPE_ALTITUDE          3060
SCOPE_LATITUDE          -24.589167
SCOPE_LONGITUDE         -70.192222

SCOPE_PSF_FILE          scao
SCOPE_STREHL_RATIO      1
SCOPE_AO_EFFECTIVENESS  100
SCOPE_JITTER_FWHM       0.001
SCOPE_DRIFT_DISTANCE    0
SCOPE_DRIFT_PROFILE     linear

SCOPE_USE_MIRROR_BG     yes

SCOPE_NUM_MIRRORS       5
SCOPE_TEMP              0
SCOPE_M1_TC             TC_mirror_EELT.dat
SCOPE_MIRROR_LIST       EC_mirrors_EELT_SCAO.tbl

################################################
```

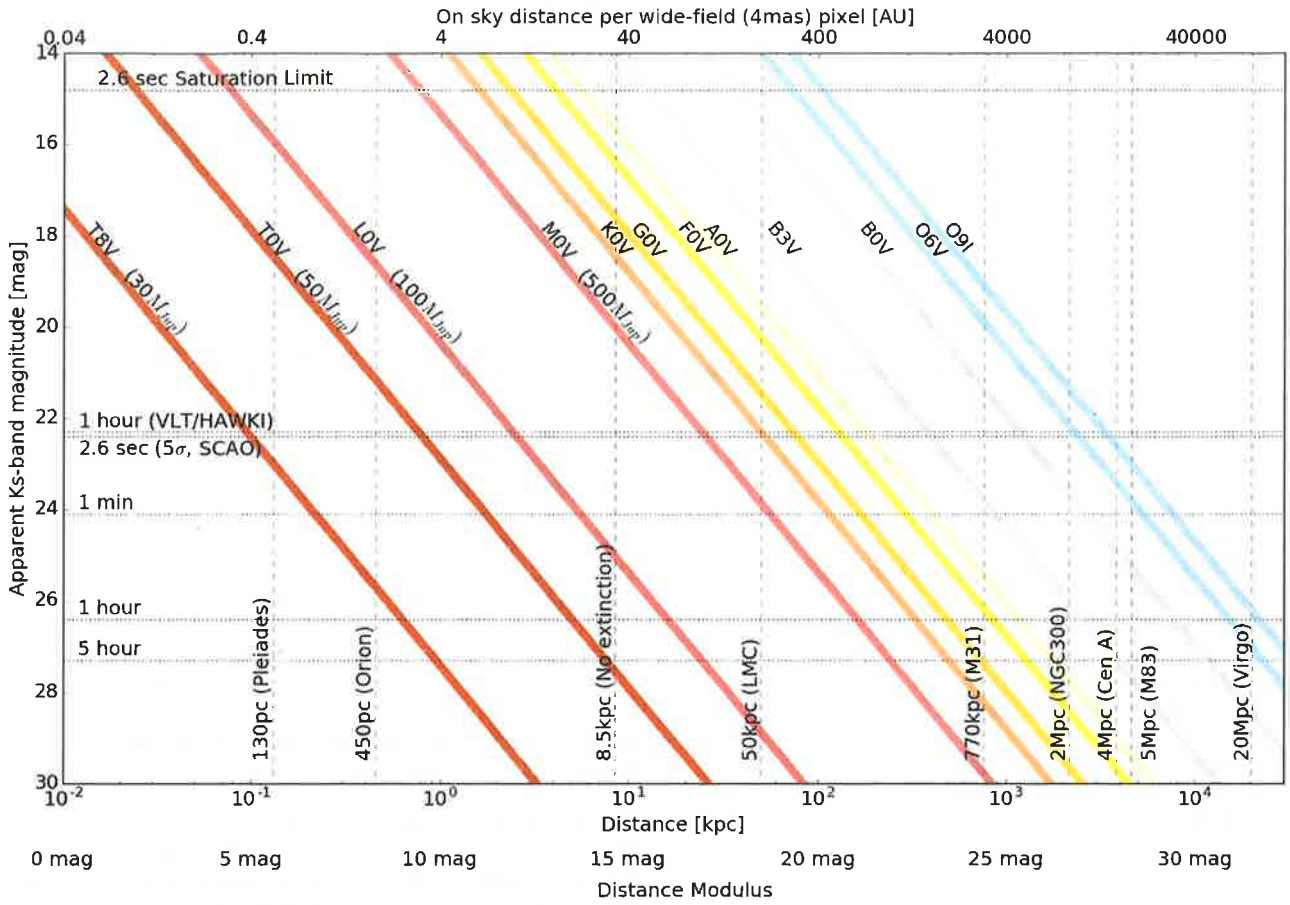

Fig. A.1. The Ks-band equivalent of Fig. 9.

```
# Instrument Parameters

INST_TEMPERATURE        -190

INST_ENTR_NUM_SURFACES  4
INST_ENTR_WINDOW_TC     TC_window.dat

INST_DICHROIC_NUM_SURFACES  2
INST_DICHROIC_TC        TC_dichroic.dat

INST_FILTER_TC          Ks

INST_PUPIL_NUM_SURFACES 2
INST_PUPIL_TC           TC_pupil.dat

# MICADO, collimator 5x, wide-field 2x (zoom 4x)
INST_NUM_MIRRORS        11
INST_MIRROR_TC          TC_mirror_gold.dat

INST_USE_AO_MIRROR_BG   yes
INST_AO_TEMPERATURE     0
INST_NUM_AO_MIRRORS     7
INST_MIRROR_AO_TC       TC_mirror_gold.dat
INST_MIRROR_AO_LIST     EC_mirrors_ao.tbl

INST_ADC_PERFORMANCE    100
INST_ADC_NUM_SURFACES   8
INST_ADC_TC             TC_ADC.dat

INST_DEROT_PERFORMANCE  100
INST_DEROT_PROFILE      linear

INST_DISTORTION_MAP     none
INST_WFE                data/INST_wfe.tbl
INST_FLAT_FIELD         none

################################################
# Spectroscopy parameters

SPEC_ORDER_SORT         HK
SPEC_SLIT_WIDTH         narrow

################################################
# Detector parameters

FPA_USE_NOISE           yes

FPA_READOUT_MEDIAN      4
FPA_READOUT_STDEV       1
FPA_DARK_MEDIAN         0.01
FPA_DARK_STDEV          0.01

FPA_QE                  TC_detector_H2RG.dat
FPA_NOISE_PATH          FPA_noise.fits
```

```
FPA_GAIN                1
FPA_LINEARITY_CURVE     FPA_linearity.dat
FPA_FULL_WELL_DEPTH     1E5

FPA_PIXEL_MAP           none
# if FPA_PIXEL_MAP == none
FPA_DEAD_PIXELS         1
FPA_DEAD_LINES          1

FPA_CHIP_LAYOUT         full
FPA_PIXEL_READ_TIME     1E-5
FPA_READ_OUT_SCHEME     double_corr

################################################
# NXRG Noise Generator package parameters
# See Rauscher (2015) for details
# http://arxiv.org/pdf/1509.06264.pdf

HXRG_NUM_OUTPUTS        64
HXRG_NUM_ROW_OH         8
HXRG_PCA0_FILENAME      FPA_nirspec_pca0.fits
HXRG_OUTPUT_PATH        none
HXRG_PEDESTAL           4
HXRG_CORR_PINK          3
HXRG_UNCORR_PINK        1
HXRG_ALT_COL_NOISE      0.5

HXRG_NAXIS1             4096
HXRG_NAXIS2             4096
HXRG_NUM_NDRO           1
```

Appendix B.2: The HAWKI configuration file

Rather than listing the full configuration for SimCADO as in Sect. B.1, we simply list the parameters that were changed in order to create an optical train for UT4/HAWKI at the VLT.

```
########################################
# Parameters regarding the "observation"

OBS_RA                  245.885625
OBS_DEC                 -26.53835
OBS_SEEING              0.6

OBS_EXPTIME             10
OBS_NDIT                1

########################################
# Parameters relating to the simulation

SIM_DETECTOR_PIX_SCALE  0.106


########################################
# Parameters regarding the telescope

SCOPE_ALTITUDE          2635
SCOPE_LATITUDE          -24.589167
SCOPE_LONGITUDE         -70.192222

SCOPE_PSF_FILE          PSF_HAWKI_poppy.fits

SCOPE_NUM_MIRRORS       3
SCOPE_M1_TC             TC_mirror_aluminium.dat
SCOPE_MIRROR_LIST       EC_hawki_vlt_mirrors.tbl


########################################
# Parameters regarding the instrument

INST_TEMPERATURE        -130
INST_ENTR_NUM_SURFACES  4
INST_FILTER_TC          TC_filter_Ks_HAWKI.dat
INST_PUPIL_NUM_SURFACES 2

INST_NUM_MIRRORS        4
INST_MIRROR_TC          TC_hawki_mirror.dat

INST_USE_AO_MIRROR_BG   no
INST_AO_TEMPERATURE     0
INST_NUM_AO_MIRRORS     0

INST_ADC_PERFORMANCE    0
INST_ADC_NUM_SURFACES   0
INST_ADC_TC             none

INST_WFE                INST_hawki_wfe.tbl


########################################
# General detector parameters

FPA_READOUT_MEDIAN      12
FPA_QE                  TC_hawki_H2RG.dat
FPA_LINEARITY_CURVE     FPA_hawki_linearity.dat
FPA_CHIP_LAYOUT         FPA_hawki_layout_cen.dat


########################################
# NXRG Noise Generator package parameters
# See Rauscher (2015) for details
# http://arxiv.org/pdf/1509.06264.pdf

HXRG_NUM_OUTPUTS        32
HXRG_NUM_ROW_OH         8
```